# Neurologic Effects of SARS-CoV-2 Transmitted among Dogs

Dong-Hwi Kim,[1] Da-Yoon Kim,[1] Kyu-Sung Kim,[1] Sang-Hoon Han, Hyeon-Jeong Go, Jae-Hyeong Kim, Kyu-Beom Lim, Dong-Hun Lee, Joong-Bok Lee, Seung-Yong Park, Chang-Seon Song, Sang-Won Lee, Yang-Kyu Choi, Yeun-Kyung Shin, Oh-Kyu Kwon, Do-Geun Kim, In-Soo Choi

SARS-CoV-2 induces illness and death in humans by causing systemic infections. Evidence suggests that SARS-CoV-2 can induce brain pathology in humans and other hosts. In this study, we used a canine transmission model to examine histopathologic changes in the brains of dogs infected with SARS-CoV-2. We observed substantial brain pathology in SARS-CoV-2–infected dogs, particularly involving blood–brain barrier damage resembling small vessel disease, including changes in tight junction proteins, reduced laminin levels, and decreased pericyte coverage. Furthermore, we detected phosphorylated tau, a marker of neurodegenerative disease, indicating a potential link between SARS-CoV-2–associated small vessel disease and neurodegeneration. Our findings of degenerative changes in the dog brain during SARS-CoV-2 infection emphasize the potential for transmission to other hosts and induction of similar signs and symptoms. The dynamic brain changes in dogs highlight that even asymptomatic individuals infected with SARS-CoV-2 may develop neuropathologic changes in the brain.

Since SARS-CoV-2 was first reported in late 2019, infection has been observed primarily in humans; however, animals of various species have also been infected, partially because their angiotensin-converting enzyme 2 (ACE2) receptor is very similar to that of humans. Infected animals show clinical signs similar to those of humans, raising concerns about potential transmission of the virus between humans and animals (*1*,*2*). SARS-CoV-2 infection in dogs and cats affects the lungs and leads to pathologic changes (Figure 1). However, whether similar pathologic manifestations occur in the brain, as observed in humans, remains unclear.

Close cohabitation of dogs and humans, and their high genetic similarity, has prompted investigations into dogs' susceptibility to SARS-CoV-2 infection (*3*,*4*). Wild-type SARS-CoV-2 infection in dogs can induce formation of neutralizing antibodies, and low viral titers in dogs demonstrate seroconversion (*5*,*6*). Mutant strains of SARS-CoV-2 in dogs cause histopathologic changes in lung tissues and increased expression of muscle damage markers in the blood (*7*). ACE2 in dogs can bind to the receptor-binding domain of SARS-CoV-2, implying the possibility of cross-species transmission between humans and dogs (*8*). Genetic and epidemiologic studies have reported animal-to-human transmission of SARS-CoV-2 (*9*).

Reportedly, SARS-CoV-2 can cause neurologic signs and symptoms (e.g., headache, fatigue, and cognitive dysfunction) in human patients. Several cohort studies report strong correlations between SARS-CoV-2 and neurologic signs/symptoms (*10*–*13*). Furthermore, cortical thickness is reduced in SARS-CoV-2–infected patients, suggesting that SARS-CoV-2 can induce pathologic changes in the brain, which may be linked to the functional deficits noted in those patients. Considering the number of patients infected with SARS-CoV-2, the neurologic signs can lead to a potential wave of neurodegenerative diseases, which could pose an immense burden on society.

The etiology of SARS-CoV-2–induced neuropathologic changes is still elusive. However, clinical and experimental reports suggest that vascular damage and the resultant immune responses in the brain may be a major factor (*13*–*16*). Magnetic resonance

Author affiliations: Konkuk University, Seoul, South Korea (D.-H. Kim, D.-Y. Kim, S.-H. Han, H.-J. Go, J.-H. Kim, K.-B. Lim, D.-H. Lee, J.-B. Lee, S.-Y. Park, C.-S. Song, S.-W. Lee, Y.-K. Choi, I.-S. Choi); Korea Brain Research Institute, Daegu, South Korea (K.-S. Kim, D.-G. Kim); Daegu Gyeongbuk Institute of Science and Technology, Daegu (K.-S. Kim, D.-G. Kim); Animal and Plant Quarantine Agency, Gimcheon, South Korea (Y.-K. Shin, O.-K. Kwon); Konkuk University Zoonotic Diseases Research Center, Seoul (D.-H. Lee, J.-B. Lee, S.-Y. Park, C.-S. Song, S.-W. Lee, I.-S. Choi); KU Center for Animal Blood Medical Science, Seoul (I.-S. Choi)

DOI: https://doi.org/10.3201/eid2911.230804

[1]These authors contributed equally to this article.

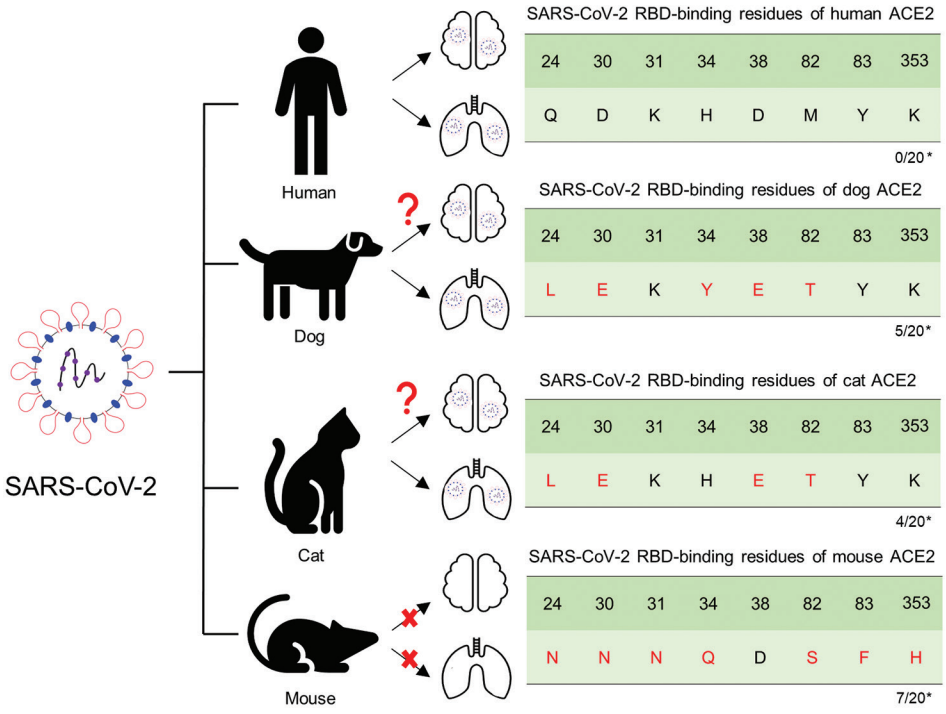


**Figure 1.** Schematic diagram representing susceptibility to SARS-CoV-2 infection in the lungs and brain of animals with potential for human transmission and homology of ACE2 amino acid sequences in study of the neurologic effects of SARS-CoV-2. *Number of mutations among the key 20 residues involved in interacting with the SARS-CoV-2 RBD. ACE2, angiotensin-converting enzyme 2; RBD, receptor-binding domain.

imaging has detected white matter hyperintensities in SARS-CoV-2–infected patients, indicating damage to the blood–brain barrier (BBB) in this region and that potentially demyelinating pathologic changes can be induced (*13*). Other studies have revealed signs of neuroinflammatory responses, including activation of microglial cells and astrocytes (*14*,*15*). Moreover, damage to the brain vasculature and defects in the coagulation system have been demonstrated (*16*). The characteristic pathologies observed in human patients (e.g., vascular damage, demyelination, and neuroinflammatory responses) have also been observed in humanized mouse models.

We used a canine transmission model to investigate the susceptibility of dogs to SARS-CoV-2, specifically the Delta variant. The dogs were housed in a Biosafety Level 3 animal facility at Konkuk University Laboratory, Seoul, South Korea, where temperature, humidity, and light were carefully controlled. The study was approved by the Animal Research Center under the supervision of the Institutional Animal Care and Use Committee (accreditation no. KU22065) and the Institutional Biosafety Committee (accreditation no. KUIBC-2022-06) at Konkuk University. The absence of SARS-CoV-2 RNA and SARS-CoV-2 antibodies in dog serum was confirmed.

## Materials and Methods

Considering that SARS-CoV-2 infections cause neurologic effects in human and human ACE2 transgenic mice, and typically follow respiratory system infection, we used models mimicking the natural infection route. We intranasally infected dogs with the Delta variant, and virus subsequently was transmitted to contact dogs. We assessed detection of viruses in the brain and damage to the integrity of the BBB as well as activation of neuroimmune responses in the brain. To test whether SARS-CoV-2 can indeed induce neuropathologic changes in the brain, we also assessed further patterns of demyelination and axonal damage. We describe our methods here in brief; details are provided in the Appendix (https://wwwnc.cdc.gov/EID/article/29/11/23-0804-App1.pdf),

We purchased fifteen 6-month-old female conventional beagles from Orient Bio, South Korea (http://www.orient.co.kr) and classified them into 3 groups: control (n = 3), infection (n = 6), and contact (n = 6). The dogs in the infection and contact groups were housed in 6 cages, each measuring 800 mm wide × 900 mm deep × 800 mm high.

To mimic natural infection, we implemented 2 infection models: intranasally inoculated dogs and dogs infected via horizontal transmission. We anesthetized 6 dogs in the infection group with 0.3 mg/kg of alfaxalone and then intranasally inoculated each dog with $10^5$ PFU of SARS-CoV-2 Delta variant. After the dogs regained consciousness and acclimated to the environment, each infected dog was placed in a cage with a dog from the contact group. To control

for any potential effects of the inoculation procedure or medium, we intranasally inoculated dogs in the control group with 500 μL of Dulbecco Modified Eagle Medium. Veterinarians visually examined the dogs for clinical signs, including neurologic signs.

With the infection model established, we next investigated the neuropathologic changes in the brain. First, we confirmed the existence of viral particles in the brain because it is logical to consider that viral particles can migrate to and replicate in the brain, which would directly damage the brain. To confirm the presence of viral nucleic acid we used quantitative reverse-transcription PCR, and to confirm the presence of viral particles we used immunofluorescence assays.

For use in additional experiments, at 4, 7, 11, 14, 18, 21, 25, 28, 32, and 35 days postinfection (dpi), we collected nasopharyngeal, oropharyngeal, and fecal swab and blood samples from all dogs while they were under sedation. At each timepoint in the early (10, 12, and 14 dpi) and late (38, 40, and 42 dpi) periods of infection, dogs were sedated and euthanized by intravenous injection of supersaturated KCl and performed necropsies (only 1 infected and 1 contact dog could be necropsied at each timepoint because of logistical constraints).

Samples underwent quantitative reverse transcription PCR, immunohistochemistry, immunofluorescence staining, ELISA, and plaque reduction neutralization test, as indicated (Appendix). We conducted all experiments in triplicate and express results as mean ±SD. We plotted dose-response curves, and we performed Student *t*-tests by using Prism 8.0.1 (Graphpad software, https://www.graphpad.com). We set statistical significance at $p<0.05$.

## Results

We detected no significant changes in objective measurements of the dogs (body weight and temperature). No dogs exhibited apparent neurologic signs or respiratory signs resembling COVID-19 (Appendix).

### Pathologic Changes in the Integrity of the BBB

In this study, we detected viral RNA in the brain during the early infection period only, not during the late infection period (Figure 2, panel A). We confirmed colocalization of the viral particles with neuronal cells

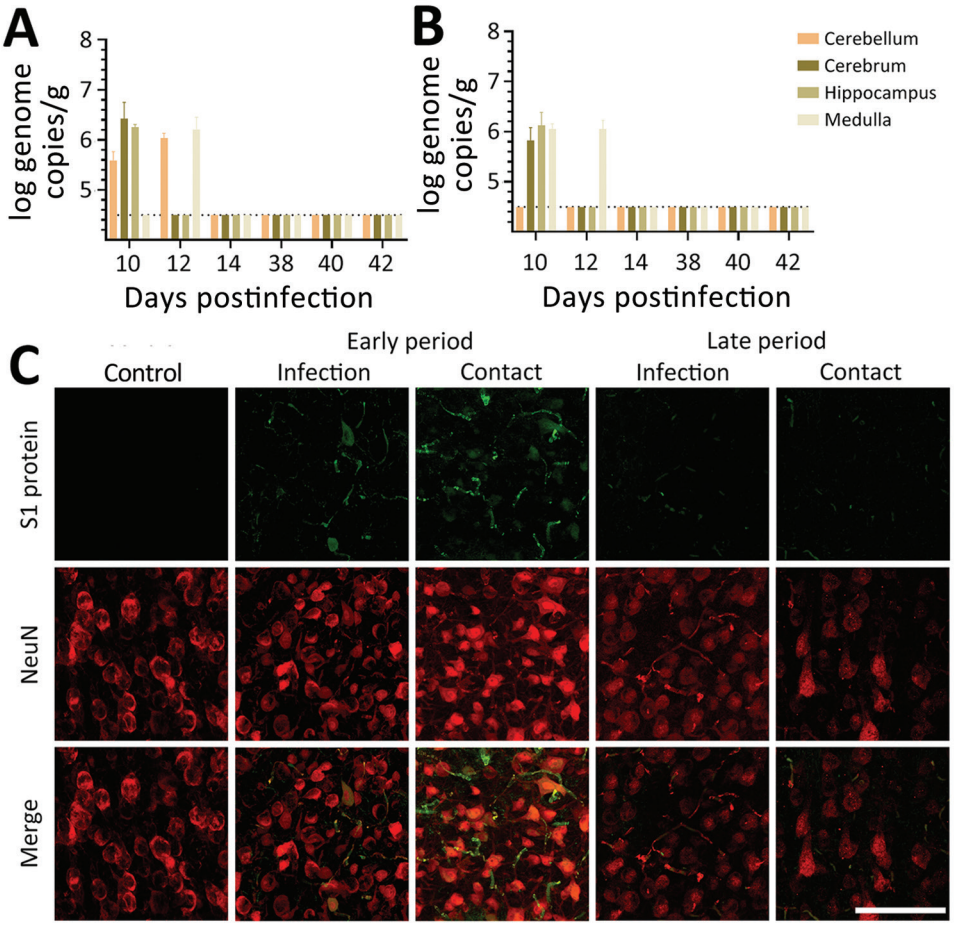


**Figure 2.** SARS-CoV-2 in the brain of dogs in study of the neurologic effects of SARS-CoV-2, showing transmission at an early stage of infection. A) Quantitative real-time PCR validation of the SARS-CoV-2 gene in the SARS-CoV-2–infected and contact groups of dogs, at each postinfection day. The dashed line indicates the regions where gene copy numbers of SARS-CoV-2 were considered negative. B) Representative fluorescent images of S1 protein (a marker of virus infection) and NeuN (a specific marker of neuronal cells) demonstrated SARS-CoV-2 infection in the canine brain sections of SARS-CoV-2–infected and contact dogs, at early and late days after infection. SARS-CoV-2–infected neuronal cells at the early stage of infection. At the late stage of infection, the presence of the virus appeared to diminish. Scale bars indicate 100 μm.

by using an immunofluorescence assay with an antibody specific to the spike protein of the virus. As for viral RNA, we also detected viral particles only during the early infection period (Figure 2, panel B). Our observations indicate that SARS-CoV-2 may infect the brain during the early infection period and may be cleared by the later infection period.

Various reports suggest damaged brain vasculature in SARS-CoV-2–infected human patients, which is reported to be associated with the influx of peripheral molecules and activation of immune responses in the brain (*13*–*16*). In our study, we tested the pathologic changes in the canine brain vasculature by using an immunofluorescence assay with antibodies specific to the BBB compartments. For dogs infected with the virus, pathologic alterations in the BBB structure were noted, showing decreased signals of matrix proteins (laminin and collagen IV) and tight junction protein (claudin 5) (Figure 3, panel A). In dogs of both groups, those phenomena were prominently observed during late rather than early infection. In addition, PDGFR-β densities, which are markers for pericytes, were decreased in dogs of both groups during the early and late periods, indicating that the cellular components of the BBB were damaged by viral infection. Moreover, the infiltrations of fibrinogen and IgG were found in the parenchyma of the brain, indicating that viral infections breached the functional integrity of the BBB (Figure 3, panel B). Last, infiltration of CD4+ T cells was found in the brain by trespassing into the BBB matrix protein layer, suggesting severe damage to the BBB integrity and subsequent recruitment of these cells into the brain (Figure 3, panels C, D). Those observations indicate that SARS-CoV-2 infection could induce pathologic changes in the structural and functional integrity of the BBB. Such changes may allow entry of peripheral molecules and immune cells into the brain parenchyma during the early infection period. Collectively, the pathologic changes concur with the typical signs of small vessel disease (SVD).

### Neuroinflammatory Responses in the Brain

When we tested whether SARS-CoV-2–induced damage of the BBB can induce neuroinflammatory responses, we stained brain sections with markers for glial activation, including glial fibrillary acidic protein and Iba-1, which are markers for activated astrocytes and microglial cells. Glial fibrillary acidic protein showed a statistically significant increase in the brain white matter of dogs in the infection and contact groups at the early and late periods, suggesting potential proinflammatory conditions in the brain (Figure 4, panel A). When we tested activation of microglial cells (another major component of innate immune responses in the brain) by staining brain sections with an antibody specific to Iba-1 (a marker of activated microglial cells), we observed a significant increase in Iba-1–positive signals in the brain white matter of dogs from both groups during the early and late periods (Figure 4, panel B). However, we did not observe such increases in the gray matter, suggesting that the microglial cell activations were specific for white matter (Figure 4, panel C). Of note, we observed activated microglial cell clustering in several spots in the white matter from dogs in both groups. Overall, those observations suggest that BBB disruption mediated by infection with SARS-CoV-2 could elicit neuroinflammatory responses and further contribute to the progression of neurodegenerative pathology in canine brains.

### Typical Signs of SVD-mediated Axonopathy

The early signs of SVD-mediated brain neurodegeneration are pathologic changes in axons and demyelination. To verify whether SARS-CoV-2 can induce these pathologic changes, we stained brain sections with antibodies against the neurofilament light chain (NFL). The intensities of NFL staining were significantly lower in the brain white matter of dogs in both groups at the early and late periods than in the uninfected control dogs (Figure 5, panels A, B). In addition, the pathologic changes in the structure and integrity of the NFL were evidenced by swelling and irregularity. Decreased NFL intensities were more severe in perivascular regions, as typical signs of SVD-mediated axonopathy.

Because demyelination is another hallmark of SVD, we assessed demyelination by using fluomyelin, a fluorescent marker for myelin. We observed a significantly lower intensity of fluomyelin in the brain white matter of dogs in the infection and contact groups during the early and late periods; NFL patterns were similar in both groups (Figure 5, panels C, D). Those changes were more evident in the perivascular area, identical to the NFL lesions. The axonopathy-like changes observed at the perivascular area of the white matter could be a consequence of SVD induction.

### Pathologic Signs of Neurodegenerative Diseases, Represented by Tauopathy

To assess production of Aβ aggregation and test whether SVD-induced neuropathologic changes can further cause neurodegenerative signs, we stained brains with an amyloid β (6E10) antibody. However, we did not observe formation of Aβ aggregates in the brains of any dogs during the early or late periods (Appendix Figure 10, panel A). Next, to assess

tauopathy in the virus-infected brains, we stained brain sections with different types of phosphorylated tau. Using a p-Tau 181 antibody, we did not observe positive signals for phosphorylated tau in any dogs (Appendix Figure 10, panel B). However, we detected phosphorylation of tau at Ser202/Thr205 by using an

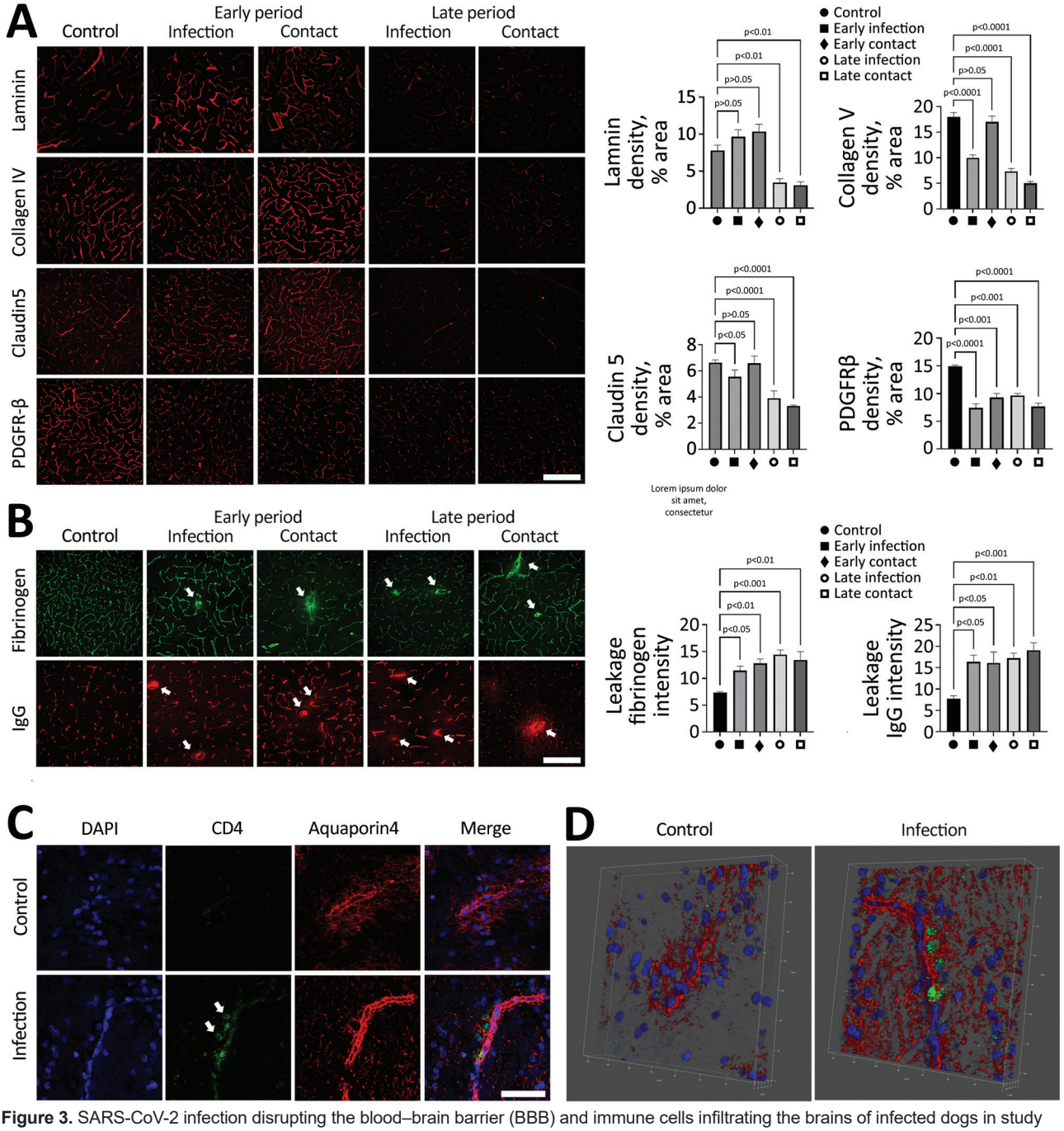


**Figure 3.** SARS-CoV-2 infection disrupting the blood–brain barrier (BBB) and immune cells infiltrating the brains of infected dogs in study of the neurologic effects of SARS-CoV-2 transmitted among dogs. A) Representative fluorescent images and statistical results of vascular markers including laminin, claudin 5, collagen IV, and PDGFR-β staining of canine brain sections derived from SARS-CoV-2–infected and contact dogs at early and late days after infection. Scale bar indicates 200 μm. B) Brain sections from SARS-CoV-2–infected and contact dogs stained with fibrinogen (green) and IgG (red), which represent BBB leakage staining, at early and late days after infection. Scale bar indicates 200 μm. (C) Representative fluorescent images of the brain sections stained with the CD4 (green) and aquaporin 4 (red), which are markers of CD4-positive T cells and astrocytic end foot, respectively. The CD4-positive cells were infiltrated in the brain parenchyma (white arrows) in the SARS-CoV-2–infected group. Scale bar indicates 50 μm. (D) Representative 3D images of CD4 (green) and aquaporin 4 (red). Statistical significance was determined using a 1-way analysis of variance. Data are presented as mean ±SEM.

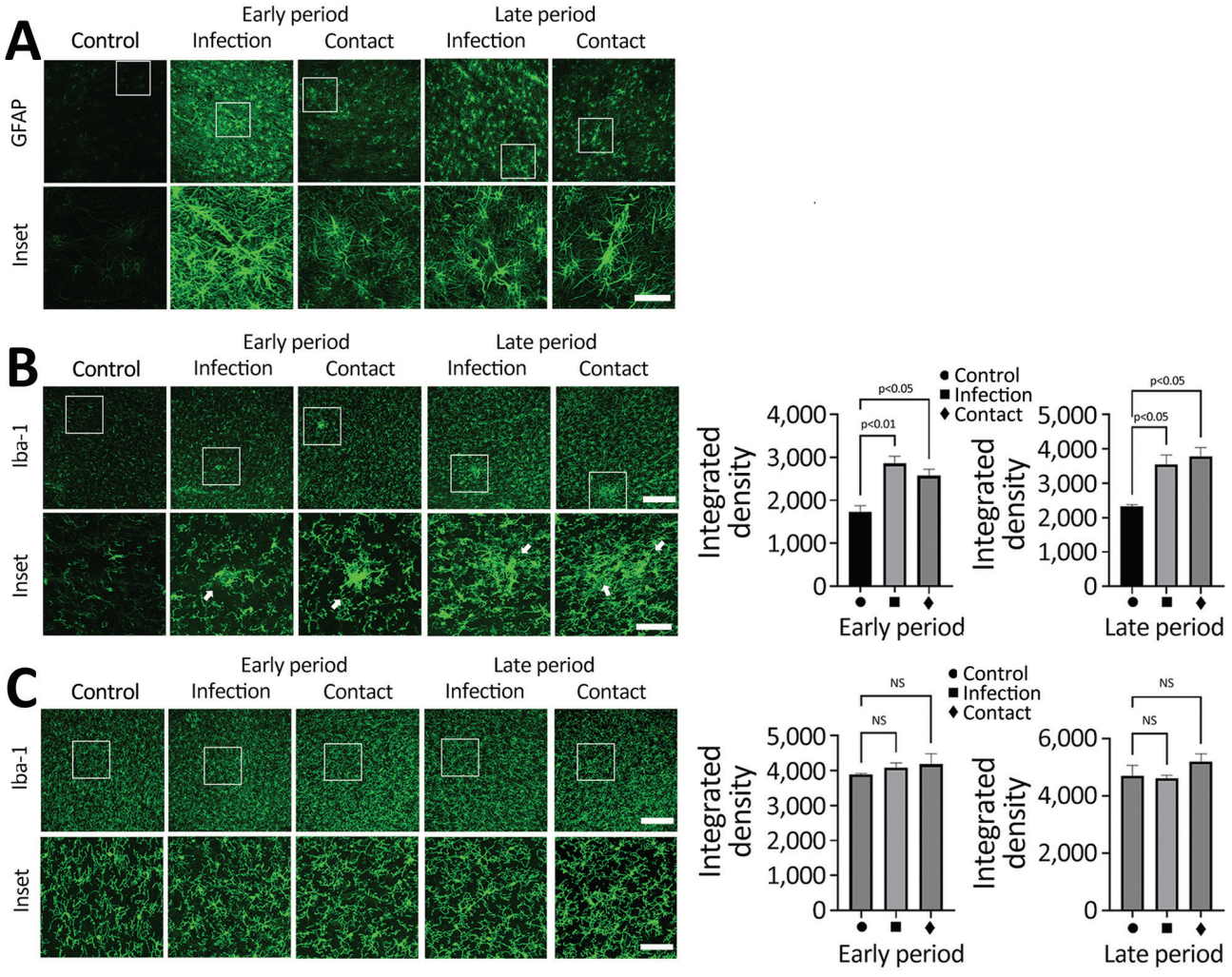


**Figure 4.** SARS-CoV-2 induces activation of microglial cells in the brain white matter in a region-specific manner in SARS-CoV-2–infected and contact dogs in study of the neurologic effects of SARS-CoV-2 transmitted among dogs. A) Representative fluorescent images of glial fibrillary acidic protein (activation astrocyte marker, green) staining of canine brain sections derived from SARS-CoV-2–infected and contact groups at early and late days after infection. Scale bars indicate 200 μm; in insets, 50 μm. B) Representative fluorescent images and statistical results of Iba-1 (a marker of microglia; green) staining of canine brain white matter sections derived from SARS-CoV-2–infected and contact dogs at early and late dpi. Scale bars indicate 200 μm; in insets, 50 μm. C) Representative fluorescent images and statistical results of Iba-1 (a marker of microglia, green) staining of canine brain gray matter sections derived from SARS-CoV-2–infected and contact dogs at early and late dpi. Scale bars indicate 200 μm; in insets, 50 μm. Statistical significance was determined using a 1-way analysis of variance. Data in graphs are presented as means ±SEM.

AT8 antibody in the brains of dogs in the infection group during the early period and dogs in the infection and contact groups during the late period. Those results suggest that SARS-CoV-2 infection could induce accumulation of the pathologic form of tau in a site-specific manner (Figure 5, panel E). Last, we used the number of neuronal cells to determine whether those pathologic neurodegenerative signatures are associated with loss of neuronal cells. We did not observe statistically significant changes in the number of cortical neurons in the brains of dogs from the infection and contact groups during the early period (Figure 5, panels F–H). However, we observed decreased numbers of neuronal cells in the infection and contact groups during the late period. Therefore, degenerative changes such as tauopathy and decreased numbers of neuronal cells in the virus-infected brains seemed to be induced after elicitation of pathologic drivers, including BBB damage, glial activation, and axonopathy, as consequences of SVD.

## Discussion

Overall, our study demonstrates solid experimental evidence that SARS-CoV-2 can infect dogs and

be transmitted to others by direct contact, producing pathologic brain changes even without prominent signs. Pathologic changes in the lung and brain were observed in dogs of both groups, providing additional evidence of virus transmission. Of note, SARS-CoV-2 infection has been reported to cause long-term pathologic effects even after the virus is cleared from the main organs of the body (*17*). Our study provides evidence that SARS-CoV-2 infection can damage the brain as well as the lungs in dogs at early and later stages of infection, suggesting a high potential for a long-lasting COVID-19–like syndrome to develop in affected dogs.

We detected SARS-CoV-2 in secretions from the nasopharynx and oropharynx of dogs in both the infection and contact groups, albeit at a low percentage. Remarkably, we found that the viral titers were higher in the nasal and oral mucosa of dogs in the contact group than in those in the infection group. That finding could be attributed to the role of the nasal and oral cavities as routes of virus entry for the contact group, resulting in higher replication of the virus at these entry points (*18*). We observed that during the early stages of infection, dogs in the contact group exhibited more severe inflammatory responses in the trachea and bronchioles than did those in the infection group. Those findings are consistent with results of previous studies that have shown that contact transmission can result in higher levels of virus titers and lead to more rapid onset of pathologic changes in the upper respiratory tract (*19*,*20*).

Seroconversion in dogs after SARS-CoV-2 infection was observed as early as 4 dpi; the rapid seroconversion may be associated with the absence of clinical signs (*21*). Antibody levels peaked a few days later in dogs in the contact group than in dogs in the infection group, suggesting later virus transmission from the virus-infected dogs. Neutralizing

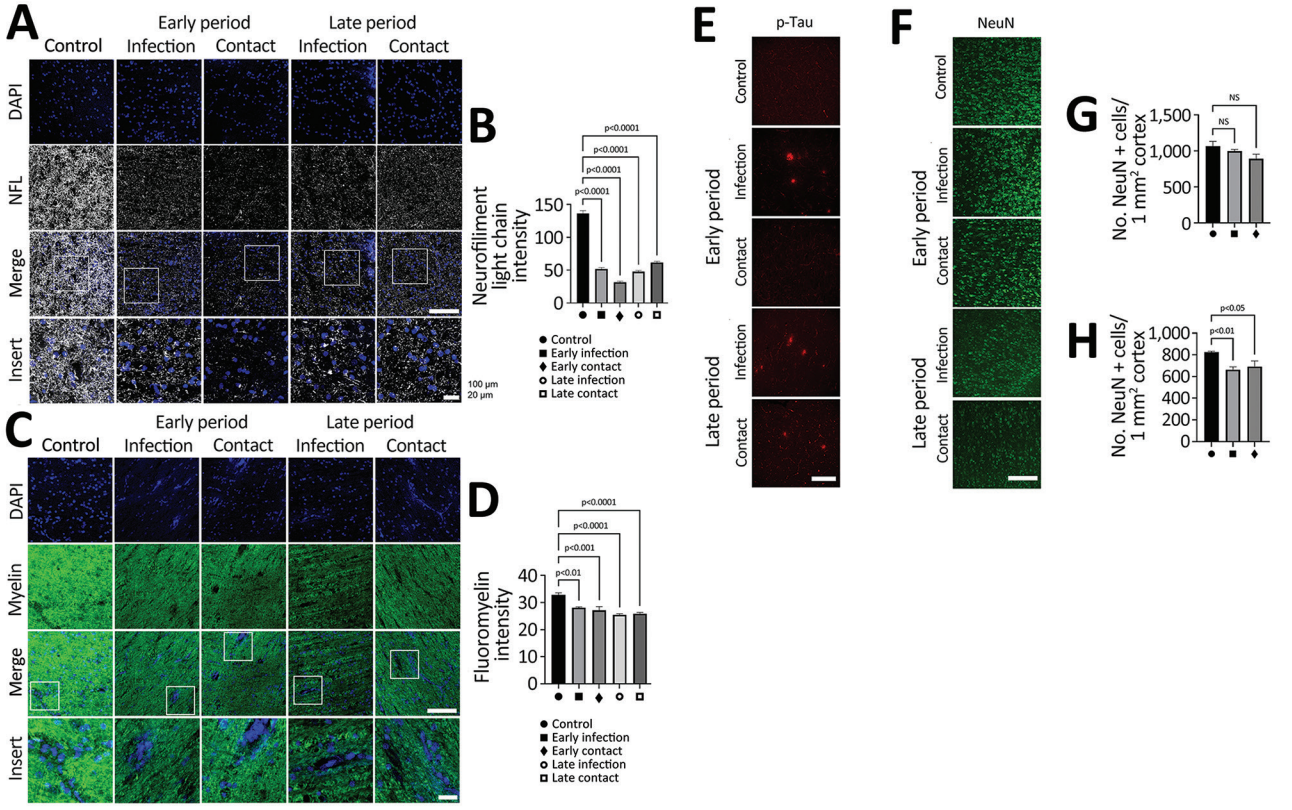


**Figure 5.** SARS-CoV-2 infection causing perivascular demyelination in the brain in dogs in study of the neurologic effects of SARS-CoV-2 transmitted among dogs. A, B) Representative fluorescent images and statistical analysis results of NFL (a marker of neurofilament light chain; gray) staining of canine brain white matter sections derived from SARS-CoV-2 infected and contact dogs at early and late dpi. Scale bar indicates 200 μm. Overall images from infected dogs demonstrate irregular axonal morphology compared with that of control dogs. Single-layer slice images. Scale bar indicates 20 μm. C, D) Representative fluorescent images and statistical analysis results of myelin (fluomyelin; green) and DAPI (blue) staining of canine brain white matter sections derived from SARS-CoV-2–infected and contact dogs at early and late dpi. Scale bar indicates 200 μm. E) Representative fluorescent images of p-tau (red) staining of canine brain gray matter sections derived from SARS-CoV-2–infected and contact dogs at early and late dpi. Scale bar indicates 200 μm. F–H) Representative fluorescent images (F) and statistical analysis results (G, H) of NeuN (a marker of neuron; green) staining of canine brain gray matter sections derived from SARS-CoV-2–infected and contact dogs at early (G) and late (H) infection. Scale bar indicates 200 μm. Statistical significance was determined using a 1-way analysis of variance. Data are presented as mean ±SEM. NS, not significant.

antibody titers against SARS-CoV-2 strongly correlate with antibody titers of the spike protein, highlighting the spike protein as a crucial target for the humoral immune response (R value >0.7; p< 0.001).

The lung alveolar septum of infected dogs was thickened overall, caused by infiltration of immune cells that indicate interstitial pneumonia (e.g., mononuclear cells, neutrophils, and macrophages) (*22*,*23*), associated with the presence of neutrophil elastase–positive cells and Iba-1–positive cells. Neutrophil elastase and Iba-1 levels increase in response to SARS-CoV-2 infection (*22*,*24*). Neutrophil elastase–positive and Iba-1–positive cells were found infiltrated around the blood vessels, indicating perivasculitis in SARS-CoV-2 infected dogs as in other hosts (*22*,*25*).

Brain damage induced by viral infection has been reported from various nonneurotrophic viruses, including HIV (*17*,*26*). Contrary to previous beliefs, accumulating evidence argues that SARS-CoV-2 can induce pathologic changes in the brains of several hosts, including humans, although the detailed mechanisms of those pathologies are still elusive. We analyzed the histopathologic changes in the brains on the basis of those uncertain arguments. Of note, we observed drastic pathologic changes in the dog brains, although the animals did not exhibit any neurologic signs**.** One of the most prominent features of brain pathology was the BBB damage observed during early infection and maintained until later infection. Typical features of vascular damage observed from SVD were changes in the level of tight junction proteins, decreased levels of laminin, and reduced pericyte coverage (*27*). SVD involves functional and structural dysfunctions of the brain vasculature, demonstrating white matter hyperintensities, microbleeding, and increased perivascular spaces. Moreover, SVD induces increased influx of peripheral blood factors and immune cells into the brain. Our finding of initial pathologic features of the BBB commonly observed in SVD in the brains of SARS-CoV-2–infected dogs strongly supports our hypothesis that the virus can induce SVD in dog brains. Several human studies supporting our observations also reported these pathologic features of the BBB similarly found in SVD (*26*,*28*,*29*).

SVD induces an influx of peripheral molecules and a favorable environment for producing large amounts of reactive oxygen species that activate microglial cells and astrocytes—hallmarks of neuroinflammatory responses. In our study, we specifically observed activation of glial cells in the white matter of the brains of the SARS-CoV-2–infected dogs, suggesting the neuroinflammatory conditions that SARS-CoV-2–mediated SVD might induce. The activation of microglial cells has also been observed in humanized ACE2 mice and brains from different animal species, including nonhuman primates (*30*,*31*). The marked axonopathy in the white matter and the preferentially increased activity of glial cells in this region strongly suggest correlations between the glial activation and development of axonopathy potentially mediated by development of SVD by SARS-CoV-2 infection. Furthermore, activation of the astrocytes and microglial cells was maintained up to 40 dpi, even when the virus was cleared from the brain. That finding strongly suggests that the glial cells activated by SARS-CoV-2 potentially harm axons or other components of neuronal cells, even when virus is absent in the brain. That topic could be the focus of future research that requires further in vitro/in vivo studies to reveal the mechanistic link between glial activation and neuronal damage mediated by SARS-CoV-2 infection.

Tau phosphorylation is the hallmark of Alzheimer's disease. Tau is the family of the microtubule-associated protein tau and functions in the delivery of synaptic vesicles required for synaptic transmission; phosphorylation of tau causes loss of this property, but the mechanism remains elusive (*32*). There are multiple phosphorylation sites on the tau protein, and our study shows the specific phosphorylation of Ser202/Thr205, detected by using the AT8 antibody (*33*). Detection of phosphorylated tau suggests a high probability of developing signs of neurodegenerative diseases in the SARS-CoV-2–infected brain. A recent study has shown the correlation between the development of SVD and the accumulation of phosphorylated tau, supporting the finding that development of phosphorylated tau could be oriented by SARS-CoV-2–associated SVD (*34*,*35*).

Long-term brain damage induced by SARS-CoV-2 has become a major topic for research of long COVID syndromes in humans (*36*). It has been reported that ≈10% of SARS-CoV-2–infected persons experience neurologic signs/symptoms, suggesting potential neurotrophic characteristics of this virus (*37*). According to recent retrospective studies that used UK Biobank data (https://www.ukbiobank.ac.uk), shrinkage in the brain cortex and decreased cognitive function have been reported for human patients after recovery from SARS-CoV-2 infection (*38*). Moreover, postmortem human brain tissue analysis demonstrated increased activity of glial cells, proinflammatory immune responses, neuronal damage, and BBB damage, enabling peripheral immune cells to infiltrate, strongly suggesting neuropathologic changes induced by SARS-CoV-2 infection (*39*). However, those pathologic changes were analyzed mainly in brain samples from patients with severe neurologic sign/symptoms;

neuropathologic changes in asymptomatic patients are still elusive. From that perspective, our study has value as translational research to predict neuropathologic changes in the early phase of asymptomatic SARS-CoV-2 infection in humans because we have observed the kinetic pathologic changes in the brains of dogs that did not show any neurologic signs. Compared with other animal models, dogs are genetically similar to humans and their brain structures are similar to those of humans, making our extrapolation more reliable. According to our results, the brains of dogs infected with SARS-CoV-2 demonstrate severe BBB disruptions and consequent SVD-like pathologic signs, including axonopathy, glial activation, and potential neurodegenerative changes even without neurologic signs. That evidence strongly suggests that even asymptomatic SARS-CoV-2 patients might have neuropathologic changes in their brains, which could develop into severe neurologic disorders later in life.

Among the merits of our study in terms of translational research of SARS-CoV-2–induced neuropathologic changes, we compared 2 infection routes: direct intranasal infection and horizontal transmission models that can mimic more natural infection routes. With that comparison, we determined that neuropathologic changes can be induced via both exposure routes, providing valuable information that owners of companion animals potentially face SARS-CoV-2–associated neurologic disorders. Second, we studied dogs, which are a more advanced species than rodents, to provide neuropathologic data that are closer to data for humans and more relevant. Moreover, our data suggest that neuropathologic changes can be induced in dogs. Last, we found that the neuroinflammatory responses were more prominently observed in the white matter area than the gray matter area, suggesting that the neuroinflammatory responses induced by SARS-CoV-2 differ by brain region. Overall, these data can be used as translational research data to interpret the potential neuropathologic changes that may be observed in humans.

This study was supported by a fund from of Animal and Plant Quarantine Agency, South Korea (project code no. Z-1543085-2022-23-02) and KBRI basic research program through Korea Brain Research Institute funded by the Ministry of Science and ICT (23-BR-04-01 to D.G.K.)

D.-H.K., D.-Y.K., and I.-S.C. conceived and validated the study. Y.-K.S. and O.-K.K. designed the study. D.-H.K., D.-Y.K., K.-S.K., S.-H.H., H.-J.G., J.-H.K., and K.-B.L. contributed to preparing and conducting the experiments. D.-H.L., J.-B.L., S.-Y.P., C.-S.S., S.-W.L., Y.-K.C., and I.-S.C. supervised the experiments. D.-H.K., D.-Y.K., K.-S.K., D.-G.K., and I.-S.C. wrote the main manuscript and prepared the figures. I.-S.C. contributed to funding acquisition. All authors reviewed the final manuscript and approved the submission. All data are presented in the paper and available from the corresponding authors on request.

## About the Author

D.-H. Kim is a PhD candidate at Konkuk University in Seoul. His primary research interests include diagnostics, vaccine development, and antiviral therapeutics, with a particular emphasis on zoonotic viruses.

## References

1. Abdel-Moneim AS, Abdelwhab EM. Evidence for SARS-CoV-2 infection of animal hosts. Pathogens. 2020;9:529. https://doi.org/10.3390/pathogens9070529
2. Mahdy MAA, Younis W, Ewaida Z. An overview of SARS-CoV-2 and animal infection. Front Vet Sci. 2020;7:596391. https://doi.org/10.3389/fvets.2020.596391
3. Lee DH, Helal ZH, Kim J, Hunt A, Barbieri A, Tocco N, et al. Severe acute respiratory syndrome coronavirus 2 (SARS-CoV-2) in a dog in Connecticut in February 2021. Viruses. 2021;13:2141. https://doi.org/10.3390/v13112141
4. Sit THC, Brackman CJ, Ip SM, Tam KWS, Law PYT, To EMW, et al. Infection of dogs with SARS-CoV-2. Nature. 2020;586:776–8. https://doi.org/10.1038/s41586-020-2334-5
5. Bosco-Lauth AM, Hartwig AE, Porter SM, Gordy PW, Nehring M, Byas AD, et al. Experimental infection of domestic dogs and cats with SARS-CoV-2: pathogenesis, transmission, and response to reexposure in cats. Proc Natl Acad Sci U S A. 2020;117:26382–8. https://doi.org/10.1073/pnas.2013102117
6. Lyoo KS, Yeo YH, Lee SG, Yeom M, Lee JY, Kim KC, et al. Susceptibility to SARS-CoV-2 and MERS-CoV in beagle dogs. Animals (Basel). 2023;13:624. https://doi.org/10.3390/ani13040624
7. Lyoo KS, Lee H, Lee SG, Yeom M, Lee JY, Kim KC, et al. Experimental infection and transmission of SARS-CoV-2 Delta and Omicron variants among beagle dogs. Emerg Infect Dis. 2023;29:782–5. https://doi.org/10.3201/eid2904.221727
8. Zhang Z, Zhang Y, Liu K, Li Y, Lu Q, Wang Q, et al. The molecular basis for SARS-CoV-2 binding to dog ACE2. Nat Commun. 2021;12:4195. https://doi.org/10.1038/s41467-021-24326-y
9. Oude Munnink BB, Sikkema RS, Nieuwenhuijse DF, Molenaar RJ, Munger E, Molenkamp R, et al. Transmission of SARS-CoV-2 on mink farms between humans and mink and back to humans. Science. 2021;371:172–7. https://doi.org/10.1126/science.abe5901
10. Xu E, Xie Y, Al-Aly Z. Long-term neurologic outcomes of COVID-19. Nat Med. 2022;28:2406–15. https://doi.org/10.1038/s41591-022-02001-z
11. Rass V, Beer R, Schiefecker AJ, Lindner A, Kofler M, Ianosi BA, et al. Neurological outcomes 1 year after COVID-19 diagnosis: a prospective longitudinal cohort study. Eur J Neurol. 2022;29:1685–96. https://doi.org/10.1111/ene.15307
12. Fleischer M, Köhrmann M, Dolff S, Szepanowski F, Schmidt K, Herbstreit F, et al. Observational cohort study of neurological involvement among patients with SARS-CoV-2 infection. Ther Adv Neurol Disord. 2021;14:1756286421993701. https://doi.org/10.1177/1756286421993701
13. Tsivgoulis G, Palaiodimou L, Zand R, Lioutas VA, Krogias C, Katsanos AH, et al. COVID-19 and cerebrovascular diseases:

a comprehensive overview. Vol. 13. In: Therapeutic Advances in Neurological Disorders. Newbury Park (CA): SAGE Publications Ltd; 2020.
14. Mirfazeli FS, Sarabi-Jamab A, Jahanbakhshi A, Kordi A, Javadnia P, Shariat SV, et al. Neuropsychiatric manifestations of COVID-19 can be clustered in three distinct symptom categories. Sci Rep. 2020;10:20957. https://doi.org/10.1038/s41598-020-78050-6
15. Shabani Z. Demyelination as a result of an immune response in patients with COVID-19. Vol. 121. In: Acta Neurologica Belgica. Berlin: Springer Science and Business Media Deutschland GmbH; 2021. p. 859–66.
16. Moonis G, Filippi CG, Kirsch CFE, Mohan S, Stein EG, Hirsch JA, et al. The spectrum of neuroimaging findings on CT and MRI in adults with COVID-19. AJR Am J Roentgenol. 2021;217:959–74. https://doi.org/10.2214/AJR.20.24839
17. Han C, Duan C, Zhang S, Spiegel B, Shi H, Wang W, et al. Digestive symptoms in COVID-19 patients with mild disease severity: clinical presentation, stool viral RNA testing, and outcomes. Am J Gastroenterol. 2020;115:916–23. https://doi.org/10.14309/ajg.0000000000000664
18. Huang N, Pérez P, Kato T, Mikami Y, Okuda K, Gilmore RC, et al. SARS-CoV-2 infection of the oral cavity and saliva. Nature Medicine. 2021;27:892–903. https://doi.org/10.1038/s41591-021-01296-8
19. Halfmann PJ, Hatta M, Chiba S, Maemura T, Fan S, Takeda M, et al. Transmission of SARS-CoV-2 in domestic cats. N Engl J Med. 2020;383:592–4. https://doi.org/10.1056/NEJMc2013400
20. Port JR. Yinda CK, Owusu IO, Holbrook M, Fischer R, Bushmaker T, et al. SARS-CoV-2 disease severity and transmission efficiency is increased for airborne compared to fomite exposure in Syrian hamsters. Nat Comm. 2021;12:1–15. https://doi.org/10.1038/s41467-021-25156-8
21. Jonczyk R, Stanislawski N, Seiler LK, Blume H, Heiden S, Lucas H, et al. Combined prospective seroconversion and PCR data of selected cohorts indicate a high rate of subclinical SARS-CoV-2 infections—an open observational study in Lower Saxony, Germany. Microbiol Spectr. 2022;10:e0151221. https://doi.org/10.1128/spectrum.01512-21
22. Patania OM, Chiba S, Halfmann PJ, Hatta M, Maemura T, Bernard KA, et al. Pulmonary lesions induced by SARS-CoV-2 infection in domestic cats. Vet Pathol. 2022;59:696–706. https://doi.org/10.1177/03009858211066840
23. Clancy CS, Shaia C, Munster V, de Wit E, Hawman D, Okumura A, et al. Histologic pulmonary lesions of SARS-CoV-2 in 4 nonhuman primate species: an institutional comparative review. Vet Pathol. 2022;59:673–80. https://doi.org/10.1177/03009858211067468
24. Kinnare N, Hook JS, Patel PA, Monson NL, Moreland JG. Neutrophil extracellular trap formation potential correlates with lung disease severity in COVID-19 patients. Inflammation. 2022;45:800–11. https://doi.org/10.1007/s10753-021-01585-x
25. Liu F, Han K, Blair R, Kenst K, Qin Z, Upcin B, et al. SARS-CoV-2 infects endothelial cells in vivo and in vitro. Front Cell Infect Microbiol. 2021;11:701278. https://doi.org/10.3389/fcimb.2021.701278
26. Barbosa-Silva MC, Santos LE, Rangel B. The impact of non-neurotropic influenza strains on the brain: a role for microglial priming? J Neurosci. 2018;38:7758–60. https://doi.org/10.1523/JNEUROSCI.1368-18.2018
27. Li Q, Yang Y, Reis C, Tao T, Li W, Li X, et al. Cerebral small vessel disease. Cell Transplant. 2018;27:1711-22. https://doi.org/10.1177/0963689718795148
28. Gyanwali B, Lui B, Tan CS, Chong EJY, Vrooman H, Chen C, et al. Cerebral microbleeds and white matter hyperintensities are associated with cognitive decline in an Asian memory clinic study. Curr Alzheimer Res. 2021;18:399–413. https://doi.org/10.2174/1567205018666210820125543
29. Østergaard L, Engedal TS, Moreton F, Hansen MB, Wardlaw JM, Dalkara T, et al. Cerebral small vessel disease: capillary pathways to stroke and cognitive decline. J Cereb Blood Flow Metab. 2016;36:302–25. https://doi.org/10.1177/0271678X15606723
30. Rutkai I, Mayer MG, Hellmers LM, Ning B, Huang Z, Monjure CJ, et al. Neuropathology and virus in brain of SARS-CoV-2 infected non-human primates. Nat Commun. 2022;13:1745. https://doi.org/10.1038/s41467-022-29440-z
31. Seehusen F, Clark JJ, Sharma P, Bentley EG, Kirby A, Subramaniam K, et al. Neuroinvasion and neurotropism by SARS-CoV-2 variants in the K18-hACE2 mouse. Viruses. 2022;14:1020. https://doi.org/10.3390/v14051020
32. Medeiros R, Baglietto-Vargas D, LaFerla FM. The role of tau in Alzheimer's disease and related disorders. CNS Neurosci Ther. 2011;17:514–24. https://doi.org/10.1111/j.1755-5949.2010.00177.x
33. Neddens J, Temmel M, Flunkert S, Kerschbaumer B, Hoeller C, Loeffler T, et al. Phosphorylation of different tau sites during progression of Alzheimer's disease. Acta Neuropathol Commun. 2018;6:52. https://doi.org/10.1186/s40478-018-0557-6
34. Kapasi A, Yu L, Petyuk V, Arfanakis K, Bennett DA, Schneider JA. Association of small vessel disease with tau pathology. Acta Neuropathol. 2022;143:349–62. https://doi.org/10.1007/s00401-021-02397-x
35. Agrawal S, Yu L, Kapasi A, James BD, Arfanakis K, Barnes LL, et al. Limbic-predominant age-related TDP-43 encephalopathy neuropathologic change and microvascular pathologies in community-dwelling older persons. Brain Pathol. 2021;31:e12939. https://doi.org/10.1111/bpa.12939
36. Washington University in St. Louis. COVID-19 infections increase risk of long-term brain problems: strokes, seizures, memory and movement disorders among problems that develop in first year after infection. Science Daily [cited 2023 Apr 10]. https://www.sciencedaily.com/releases/2022/09/220922124408.htm
37. Ozel T, Erdem NS, Ünal A, Yalçin AN, İnan D, Ilhanli N, et al. Neurological manifestations and mortality in hospitalized coronavirus disease 2019 patients. Neurological Sciences and Neurophysiology. 2022;39:138–145. http://doi.org/10.4103/nsn.nsn_117_21
38. Douaud G, Lee S, Alfaro-Almagro F, Arthofer C, Wang C, McCarthy P, et al. SARS-CoV-2 is associated with changes in brain structure in UK Biobank. Nature. 2022;604:697–707. https://doi.org/10.1038/s41586-022-04569-5
39. Matschke J, Lütgehetmann M, Hagel C, Sperhake JP, Schröder AS, Edler C, et al. Neuropathology of patients with COVID-19 in Germany: a post-mortem case series. Lancet Neurol. 2020;19:919–29. https://doi.org/10.1016/S1474-4422(20)30308-2

Address for correspondence: In-Soo Choi, Konkuk University, Veterinary Infectious Diseases, #1 Hwayang-dong Gwanjin-gu, Seoul 143-701, South Korea; email: ischoi@konkuk.ac.kr;
Do-Geun Kim, Dementia Research Group, Korea Brain Research Institute, 61 Cheomdaro, Sinseo, Donggu, Daegu, South Korea; email: kimvet0911@kbri.re.kr

Article DOI: https://doi.org/10.3201/eid2911.230804



# Neurologic Effects of SARS-CoV-2 Transmitted among Dogs

## Appendix

## MATERIALS AND METHODS

### Virus amplification, experimental design, and sample collection

SARS-CoV-2 delta variant (GK clade, AY.69 lineage, NCCP No. 43409) was obtained from the National Culture Collection for Pathogens in South Korea. The virus was amplified on Vero76 cells and titrated using plaque forming assay. The dogs were classified into three groups: MOCK (n = 3), infection (n = 6), and contact (n = 6). The dogs in the infection and contact groups were housed in six cages, with each cage measuring 800W × 900D × 800H mm. One dog from the infection group and one dog from the contact group were kept together in each cage. Six dogs in the infection group were anesthetized with 0.3 mg/kg of alfaxalone (Alfaxan® Multidose, Jurox, Australia) and then inoculated with $10^5$ PFU of SARS-CoV-2 delta variant through the nasal cavity. After regaining consciousness and acclimating to the environment, each infected dog was placed one-on-one in a cage with a dog from the contact group. The MOCK control group was inoculated with 500 μL of Dulbecco's Modified Eagle Medium into the nasal cavity to control for any potential effects of the inoculation procedure or medium. The clinical signs, including neurological signs in the dogs, were visually evaluated by veterinarians. At 4-, 7-, 11-, 14-, 18-, 21-, 25-, 28-, 32-, and 35-days post-infection (dpi), nasopharyngeal, oropharyngeal, and fecal swabs, as well as blood samples, were collected from all dogs under sedation for further experiments. At the early (10, 12, and 14 dpi) and late (38, 40, and 42 dpi) periods of infection, the dogs were euthanized by intravenous injection of supersaturated KCl under sedation, and autopsies were performed. Due to logistical constraints, only one infected and one contact dog was autopsied daily.

### Statistical analysis

All experiments were conducted in triplicate and are expressed as the mean ± SD. Dose-response curves were plotted, and Student's t-tests were performed using PRISM 8.0.1 (Graphpad Software, CA); statistical significance was set at $p < 0.05$.

### Chemicals and Reagents

The following antibodies were used: anti-fibrinogen (1:500, Dako, A0080), anti-Dog IgG (IFA; 1:500, Invitrogen, SA5-10309), anti-Dog IgG (ELISA; 1:1000, GeneTex, GTX77013), Dog IgM (1:1000, GeneTex, GTX77081), anti-Dog IgA (1:1000, GeneTex, GTX77075), HRP-conjugated anti-Goat IgG (1/5000, Abcam, ab97110), anti-NeuN (1:500, CST, 12943s), anti-SARS-CoV-2 spike protein (1:500, Invitrogen, MA5-36247), anti-GFAP (1:500, CST, 3670s), anti-neutrophil elastase (1:200, Abcam, ab68672), anti-Iba-1 (1:500, FUJIFILM, 019-19741), anti-FluoroMyelin (1:500, Invitrogen, F34652), anti-NFL (1:500, CST, 2837s), anti-phospho Tau (1:500, Thermo, MN1020), anti-6E10 (1:500, Bio-legend, 803001), anti-CD31 (1:100, MyBiosource, MBS249056), anti-AQP4 (1:500, CST, 59678), anti-Laminin (1:500, Abcam, ab11575), anti-Claudin5 (1:500, Invitrogen, 35-2500), anti-Collagen IV (1:500, Abcam, ab6586), anti-PDGFRβ (1:500, CST, 3169s), and CD4 (1:100 dilution, R&D system, MAB2410). The following recombinant antigens were used: recombinant SARS-CoV-2 spike S1 protein (GeneTex, GTX135817-pro) and recombinant SARS-CoV-2 nucleocapsid protein (GeneTex, GTX135357-pro).

### Reverse transcription-quantitative polymerase chain reaction (RT–qPCR)

Nasopharyngeal, oropharyngeal, and fecal swabs were resuspended in 150 μL of phosphate-buffered saline (PBS). Blood samples were collected using BD Vacutainer® SST™II Advance (BD, UK) and centrifuged at 3,000 × *g* to obtain serum samples. Viral RNA was extracted from the nasopharyngeal, oropharyngeal, and fecal swabs, and serum using the RNeasy Mini RNA isolation kit (Qiagen, Germany), following the manufacturer's instructions. RNA from canine tissue was extracted using the TRIzol reagent (Invitrogen, 15596018). Chloroform was added to the mixture and then centrifuged at 12,000 × *g* for 15 min. The supernatant was combined with isopropanol at a ratio of 1:1 and incubated at room temperature for 10 min. The mixture was centrifuged at 12,000 × *g* for 10 min, and the supernatant was discarded. The RNA pellet was washed twice with 75% ethanol in nuclease-free water. The ethanol was removed, and the pellet was air-dried for 10 min. The RNA pellet was resuspended in 30 μL of nuclease-free

water and reverse transcribed using the High-Capacity cDNA Reverse Transcription kit with RNase inhibitor (ABI, 4374966). Real-time RT-qPCR was conducted using the KAPA SYBR FAST kit (Roche, KK4602). The PCR mixture contained KAPA SYBR FAST qPCR Master Mix (2X) Universal, gene-specific primers for the SARS-CoV-2 M gene, and 50X ROX High. Thereafter, 20 ng of cDNA product was diluted in the PCR mixture. Amplification was performed using the QuantStudio 5 machine. Thermal cycling conditions consisted of pre-incubation at 95°C for 3 min, followed by 40 cycles of amplification at 95°C for 10 s. The melting temperature of the PCR product was determined via melting curve analysis, which was performed by heating the PCR product from 65°C to 97°C and then cooling it at 40°C for 10 s. The viral GE copy numbers were calculated from a standard curve generated with plasmid DNA containing the target sequence of the M gene. The relative fold changes in control, infection, and contact groups were calculated using the comparative threshold cycle method. The following gene sequences were used in this study: SARS-CoV-2 M gene: Forward primer, 5′-GGYTCTAARTCACCCATTCA -3′; Reverse primer, 5′-TGATACTCTARAAAGTCTTCATA -3′

#### Immunohistochemistry (IHC)

IHC was performed for Iba-1 and neutrophil elastase. Formalin-fixed, paraffin-embedded tissues were processed into 5 μm sections and mounted on silane-coated slides. The sections were then deparaffinized in xylene, rehydrated in graded ethanol, and washed with distilled water (DW). Antigen retrieval was achieved by pressurizing the sections in Na-citrate buffer (pH 6.0) for 10 min, followed by cooling in iced water and washing thrice with PBS. Thereafter, the sections were incubated with 3% hydrogen peroxide prepared in methanol for 10 min at room temperature to block endogenous hydrogen peroxidase activity. After washing thrice with PBS, the sections were treated with normal goat serum (Vectastain Elite ABC-HRP Kit, Peroxidase (Rabbit IgG); Vector Laboratories, US) for 30 min to block non-specific binding of antibodies. The sections were then treated with the primary antibodies and incubated overnight at 4°C (see Table 1 for details). The sections were washed thrice with PBS, incubated with biotinylated goat anti-rabbit IgG (Vectastain Elite ABC-HRP Kit, Peroxidase (Rabbit IgG); Vector Laboratories, US) for 1 h at room temperature, rewashed thrice with PBS, and incubated with ABC reagent (Vectastain Elite ABC-HRP Kit, Peroxidase (Rabbit IgG); Vector Laboratories, US) for 30 min at room temperature. The primary antibody, biotinylated secondary antibody, and avidin-biotin

horseradish peroxidase complex were visualized using the DAB/Ni peroxidase substrate kit (Vector Laboratories, US). Finally, the sections were counterstained with Gill's Hematoxylin II, dehydrated in graded alcohol series, and mounted.

#### Immunofluorescence staining

The brains were fixed in 4% paraformaldehyde (PFA) overnight and incubated in 30% sucrose for 48 h before embedding and freezing in an optimal cutting-temperature compound (Tissue-Tek). Brain sections were cut into 20 μm sections and stored at −20°C. Before immunostaining, the slides were permeabilized with 1% Triton X-100 in PBS for 20 min and blocked with 5% normal goat serum in PBS for 1 h. For immunostaining of the brain vascular and peripheral immune cells, the canine brain tissues were sectioned to 50 μm, maintained in 0.5% $NaH_2PO_4$ until use, and stored at 4°C. Antigen retrieval was performed by incubating the sections in citrate buffer, pH 6.0, at 80℃ for 30 min. Primary antibodies were diluted in 1% Triton X-100 in PBS containing 5% normal goat serum and incubated overnight at room temperature. The following day, the slides were washed five times in dPBSm, incubated with fluorescently conjugated secondary antibodies for 1 h at room temperature, and diluted 1:500 fold in 5% normal goat serum in PBS. After washing with dPBS, the slides were counterstained with DAPI and coverslipped with Fluoromount-G (Electron Microscopy Science). Images were acquired with a Leica Confocal microscope (SP8) and reconstructed using LAS X software with maximal projection intensity (MPI).

#### Enzyme-linked immunosorbent assay (ELISA)

Antibody titers specific for the SARS-CoV-2 S protein and N protein were determined using ELISA. Serum samples were diluted 1000-fold for IgG and 10000-fold for IgM and IgA and then transferred to microplate wells coated with recombinant SARS-CoV-2 S protein or N protein at a concentration of 0.2 μg/mL. After washing five times with PBS, the plate was incubated with anti-IgG, anti-IgM, or anti-IgA antibodies for 1 h and 30 min. After washing five times with PBS, the plate was incubated with 5000-fold-diluted HRP-conjugated anti-goat IgG for 1 h. After washing five times with PBS, the colorimetric reaction was initiated by adding tetramethylbenzidine (TMB) and terminated by adding 2M H2SO4. Optical density (OD) was measured at 450 nm using an ELISA reader.

### Plaque reduction neutralization test

Neutralizing antibodies were detected by performing a plaque reduction neutralization test. In this assay, serum was diluted 10-fold, and 50 μL of the diluted serum was mixed with 30 PFU/50 μL of the SARS-CoV-2 delta variant. The mixture was then incubated at 37°C for 1 h and transferred to a 6-well plate containing cells at 90% confluency. The cells were infected with the virus mixture for 1 h and washed thrice with PBS. The cells were overlaid with 2% DMEM and 0.6% agarose. After four days of infection, the number of plaques caused by viral infection was counted, and the plaques formed in the presence of serum from the negative control group were compared. The presence of neutralizing antibodies was confirmed if the percentage of plaques formed in the presence of serum from the experimental group was lower than that of the negative control group. Data are presented as mean ± SD.

## Establishment and verification of canine SARS-CoV-2 infection and transmission model

SARS-CoV-2 RNA was detected in nasopharyngeal and oropharyngeal swabs of both groups from 4–14 days post-infection (dpi). All dogs in both groups had detectable SARS-CoV-2 RNA in their serum and feces at 14 dpi, and in some dogs, the virus persisted until 18 dpi (Appendix Figure 1). Clinical signs such as weight loss, increased body temperature, and cough were carefully monitored during the experimental period. However, all dogs showed no clinical signs of COVID-19 (Appendix Figure 2). To confirm the distribution of SARS-CoV-2 in the lungs, lung tissue samples were collected through autopsy from an infected dog and a contact dog on a determined day at two different periods set as an early period (10, 12, and 14 dpi) and a late period (38, 40, and 42 dpi) of infection. Six lung lobes were collected from each dog. SARS-CoV-2 RNA was detected in two dogs during the early infection period: one in the infected dog (10 dpi, right accessory lobe) and one in the contact dog (12 dpi, right cranial and left cranial lobes). Immunohistochemical analysis of the viral-positive tissues revealed the presence of viral antigens (Appendix Figure 3).

The histopathological changes were confirmed in the lung tissues obtained from dogs in both infection and contact groups. The alveolar septa of the lung tissues in all dogs were thickened by interstitial infiltration of inflammatory cells (neutrophil elastase$^+$ or Iba-1$^+$ cells)

during the early infection period, which persisted to the late period (Appendix Figure 4, panel A, and Appendix Tables 1 and 2). The percentage of parenchymal tissue in the lungs was calculated by the methods described in Appendix Figure 5. The analysis was performed on randomly selected zones within the six lobes of the lungs obtained from all individuals. All experimental groups exhibited a significant increase in lung parenchymal areas compared with the negative control group. The parenchymal areas in the infection group dogs were significantly wider during the late infection period than in the early period. The parenchymal areas of the contact group were larger in the early infection period than in the late period (Appendix Figure 4, panel B, and Appendix Table 3). Lesions exhibiting thickened alveolar septa were confirmed to have infiltration of neutrophils and other mononuclear cells, considered a diagnostic marker of interstitial pneumonia (Appendix Figure 4, panel C). Distinct histopathological changes were evident in the dogs of the contact group, including bronchus-associated lymphoid tissue (BALT), which may have been formed through antigen priming in the early infection period. Furthermore, inflammatory cell infiltration was observed in the trachea and bronchiole tissues. In the late period, there was evidence of infiltration by neutrophil elastase-positive cells or Iba-1-positive cells in those tissues of the contact group dogs (Appendix Figure 6). The infiltrated inflammatory cells were observed around the pulmonary blood vessels in the infection and contact groups. This phenomenon was observed during both the early and late infection periods. Immunostaining analysis confirmed the involvement of neutrophil elastase-positive cells and Iba-1-positive cells in the perivascular inflammatory response (Appendix Figure 7).

## Serological evidence of humoral immune response to SARS-CoV-2 infection in dogs

To further investigate whether there were immunological changes in response to viral infection, we examined the formation of humoral immunity against SARS-CoV-2. For this, antibody tests for anti-SARS-CoV-2 IgM, IgG, and IgA were conducted using ELISA after coating SARS-CoV-2 spike (S) and nucleocapsid (N) proteins to determine seroconversion to SARS-CoV-2 infection in both groups. In the infected group, anti-S IgM levels peaked at 11 dpi and decreased afterward, whereas the peak and subsequent decrease were approximately 14 dpi in the contact group. Anti-S IgG was also detected from 4 dpi, and its levels remained high until 35 dpi, unlike anti-S IgM, which declined after the early period. The blood anti-S IgA of the

experimental group showed higher antibody values than that of the MOCK group. However, anti-S IgA exhibited relatively low OD values compared with anti-S IgM and IgG (Appendix Figure 8, panel A). Anti-N antibodies showed a similar trend to that of anti-S antibodies but with a higher background signal (Appendix Figure 8, panel B). These results demonstrate that seroconversions effectively occurred in dogs from both groups—intranasally infected with the SARS-CoV-2 delta variant and contacted from the infected dogs. The neutralizing activities of the serum antibodies against the SARS-CoV-2 delta variant were determined with 10-fold serially diluted serum samples. A decrease in plaque formation was observed in all infected and contact dogs, indicating that the antibodies present in the serum possess neutralizing ability against the virus (Appendix Figure 8, panel C). The plaque reduction rates of the infection group were over 60% in all dogs except one at 7 dpi, while the highest reduction rates observed in the contact group were only 32.63% on average. By 28 dpi, all dogs in both groups showed more than 90% plaque inhibition (Appendix Table 4). When a correlation between the plaque reduction ability and the anti-S Ig or anti-N IgG was analyzed, the reduction of plaque formation was significantly associated with anti-S IgG but not anti-N IgG titers (Appendix Figure 9). By conducting these verification procedures, we established that this infection model is suitable for analyzing neuropathological changes in the canine brain.

**Appendix Table 1.** Comparison of Iba-1 positive ratios between five study groups: results of t-tests

| **Group** (Mean ± SD) | **MOCK** (1.599 ± 1.015) | **Infection, Early period** (4.248 ± 2.626) | **Contact, Early period** (3.272 ± 0.983) | **Infection, Late period** (4.950 ± 3.092) | **Contact, Late period** (4.227 ± 3.527) |
|---|---|---|---|---|---|
| **MOCK** (1.599 ± 1.015) | - | ** $p = 0.0025$ | *** $p < 0.001$ | ** $p = 0.0011$ | * $p = 0.0185$ |
| **Infection, Early period** (4.248 ± 2.626) | ** $p = 0.0025$ | - | $p = 0.1491$ | $p = 0.4682$ | $p = 0.9842$ |
| **Contact, Early period** (3.272 ± 0.983) | *** $p < 0.001$ | $p = 0.1491$ | - | * $p = 0.0352$ | $p = 0.2762$ |
| **Infection, Late period** (4.950 ± 3.092) | ** $p = 0.0011$ | $p = 0.4682$ | * $p = 0.0352$ | - | $p = 0.5180$ |
| **Contact, Late period** (4.227 ± 3.527) | * $p = 0.0185$ | $p = 0.9842$ | $p = 0.2762$ | $p = 0.5180$ | - |

*$p < 0.05$, **$p < 0.01$, and ***$p < 0.001$

**Appendix Table 2.** Comparison of neutrophile elastase positive ratios between five study groups: results of t-tests

| **Group** (Mean ± SD) | **MOCK** (3.285 ± 1.905) | **Infection, Early period** (7.441 ± 4.937) | **Contact, Early period** (7.581 ± 3.852) | **Infection, Late period** (10.444 ± 4.109) | **Contact, Late period** (10.744 ± 7.165) |
|---|---|---|---|---|---|
| **MOCK** (3.285 ± 1.905) | - | ** $p = 0.0099$ | ** $p = 0.0013$ | *** $p < 0.001$ | ** $p = 0.0016$ |
| **Infection, Early period** (7.441 ± 4.937) | ** $p = 0.0099$ | - | $p = 0.9254$ | $p = 0.05545$ | $p = 0.1166$ |
| **Contact, Early period** (7.581 ± 3.852) | ** $p = 0.0013$ | $p = 0.9254$ | - | * $p = 0.0382$ | $p = 0.1082$ |
| **Infection, Late period** (10.444 ± 4.109) | *** $p < 0.001$ | $p = 0.05545$ | * $p = 0.0382$ | - | $p = 0.8787$ |
| **Contact, Late period** (10.744 ± 7.165) | ** $p = 0.0016$ | $p = 0.1166$ | $p = 0.1082$ | $p = 0.8787$ | - |

*$p < 0.05$, **$p < 0.01$, and ***$p < 0.001$

**Appendix Table 3**. Comparison of lung parenchymal area ratios between five study groups: results of t-tests

| **Group** (Mean ± SD) | **MOCK** (18.467 ± 9.573) | **Infection, Early period** (35.133 ± 10.333) | **Contact, Early period** (54.540 ± 13.834) | **Infection, Late period** (45.102 ± 8.331) | **Contact, Late period** (34.673 ± 18.217) |
|---|---|---|---|---|---|
| **MOCK** (18.467 ± 9.573) | - | *** $p < 0.001$ | *** $p < 0.001$ | *** $p < 0.001$ | ** $p = 0.0087$ |
| **Infection, Early period** (35.133 ± 10.333) | *** $p < 0.001$ | - | *** $p < 0.001$ | ** $p = 0.0031$ | 0.9264 |
| **Contact, Early period** (54.540 ± 13.834) | *** $p < 0.001$ | *** $p < 0.001$ | - | * $p = 0.0183$ | *** $p < 0.001$ |
| **Infection, Late period** (45.102 ± 8.331) | *** $p < 0.001$ | ** $p = 0.0031$ | * $p = 0.0183$ | - | * $p = 0.0340$ |
| **Contact, Late period** (34.673 ± 18.217) | ** $p = 0.0087$ | 0.9264 | *** $p < 0.001$ | * $p = 0.0340$ | - |

*$p < 0.05$, **$p < 0.01$, and ***$p < 0.001$

**Appendix Table 4**. Reduction in SARS-CoV-2-specific plaque formation rates via neutralized antibodies derived from the infected and contact groups of dogs

| | | **Days post infection (dpi)** | | | | |
|---|---|---|---|---|---|---|
| **Group** | **Dog number** | **7 dpi** | **14 dpi** | **21 dpi** | **28 dpi** | **35 dpi** |
| Infection | Infected dog 1 | 69.47 ± 0.05% | 93.75 ± 0.02% | 96.77 ± 0.03% | 92.47 ± 0.04% | 96.67 ± 0.03% |
| | Infected dog 2 | 69.47 ± 0.06% | 89.06 ± 0.08% | 92.47 ± 0.05% | 93.55 ± 0.03% | 94.44 ± 0.04% |
| | Infected dog 3 | 32.63 ± 0.06% | - | - | - | - |
| | Infected dog 4 | 64.21 ± 0.08% | 93.75 ± 0.06% | - | - | - |
| | Infected dog 5 | 91.58 ± 0.04% | 93.75 ± 0.02% | 95.70 ± 0.04% | 96.77 ± 0.03% | 96.67 ± 0.03% |
| | Infected dog 6 | 84.21 ± 0.03% | - | - | - | - |
| Contact | Contacted dog 1 | 3.16 ± 0.06% | 85.94 ± 0.04% | 88.17 ± 0.04% | 95.70 ± 0.04% | 92.22 ± 0.07% |
| | Contacted dog 2 | 4.21 ± 0.05% | 79.69 ± 0.06% | 91.40 ± 0.02% | 98.92 ± 0.02% | 93.33 ± 0.07% |
| | Contacted dog 3 | 6.32 ± 0.04% | - | - | - | - |
| | Contacted dog 4 | 5.26 ± 0.03% | 3.13 ± 0.08% | - | - | - |
| | Contacted dog 5 | 28.42 ± 0.05% | 76.56 ± 0.04% | 89.25 ± 0.05% | 97.85 ± 0.02% | 85.56 ± 0.04% |
| | Contacted dog 6 | 32.63 ± 0.05% | - | - | - | - |

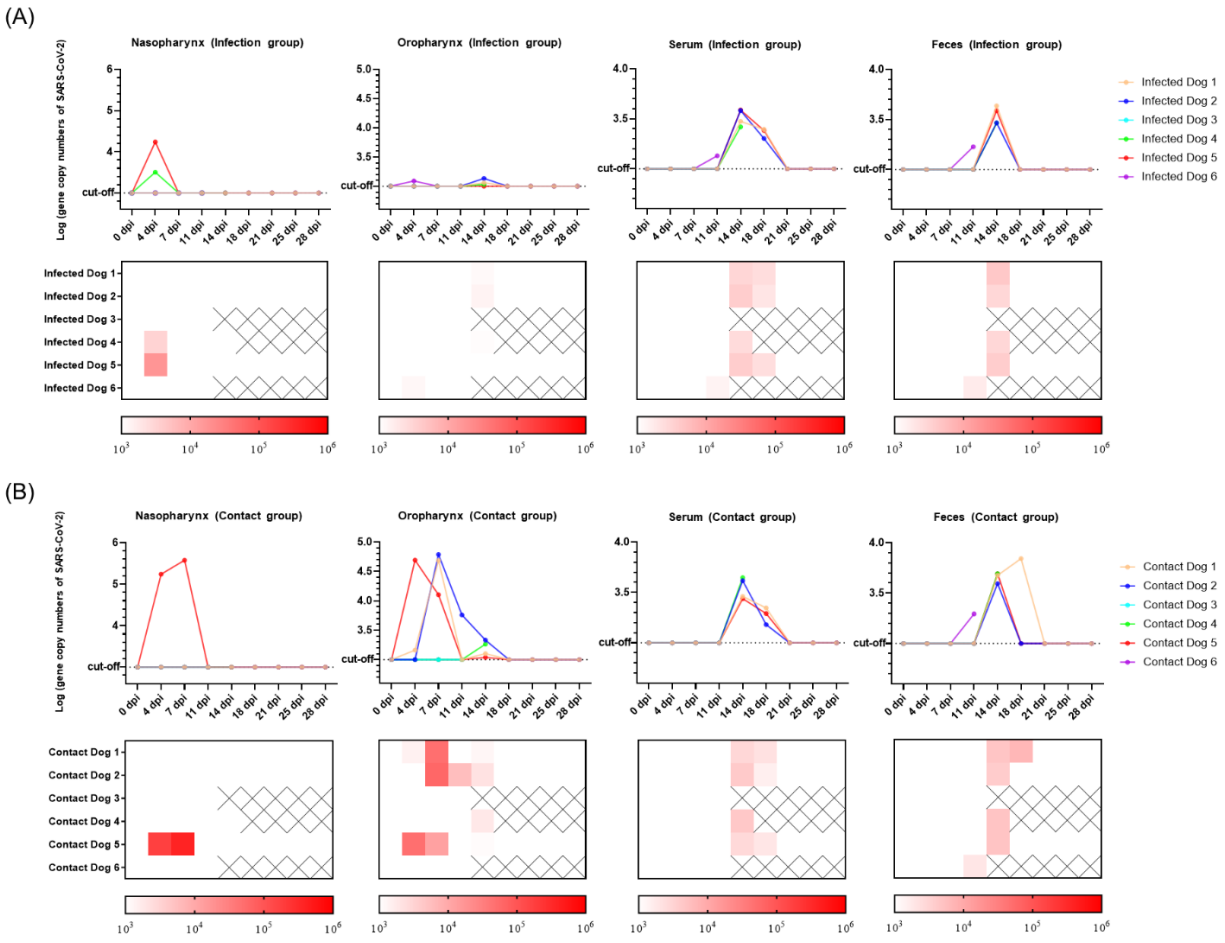


**Appendix Figure 1.** Detection of SARS-CoV-2 in the nasopharyngeal, oropharyngeal, and fecal swabs, and serum of infected and contact dogs for 28 days post-infection. Serum, fecal, nasopharyngeal, and oropharyngeal swabs were collected periodically from all dogs following virus inoculation. After the inactivation process (55°C, 30 min), the samples underwent further analysis for viral RNA using RT-qPCR. The Ct value corresponding to the lowest detectable copy number on the standard curve, where the fluorescence signal exceeds the background noise, was set as the cut-off value. Additionally, heat maps are presented below the line graphs to facilitate better comprehension of the same results.

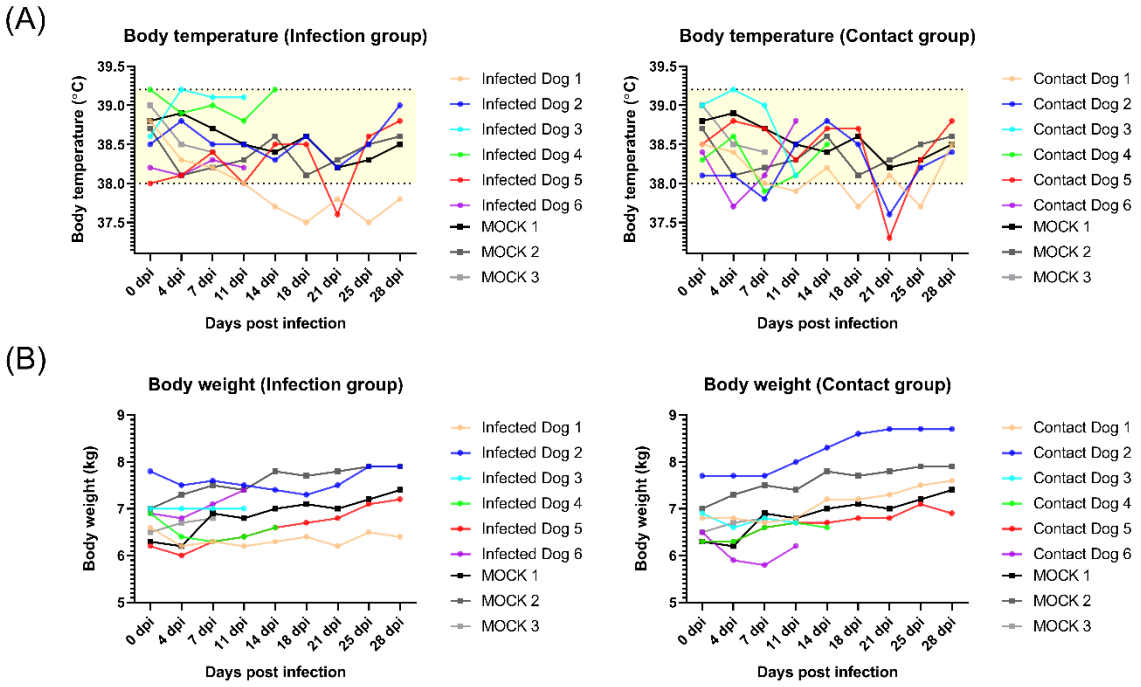


**Appendix Figure 2.** Changes in body temperature and weight of SARS-CoV-2-infected and contact dogs. (A) Body temperature was measured via rectal thermometry. No dogs with high fever were observed during the experiment; however, some dogs exhibited mild hypothermia. The normal body temperature range for dogs was established as 38.0–39.2°C and highlighted in a yellow box. (B) No significant changes in weight were observed after SARS-CoV-2 infection.

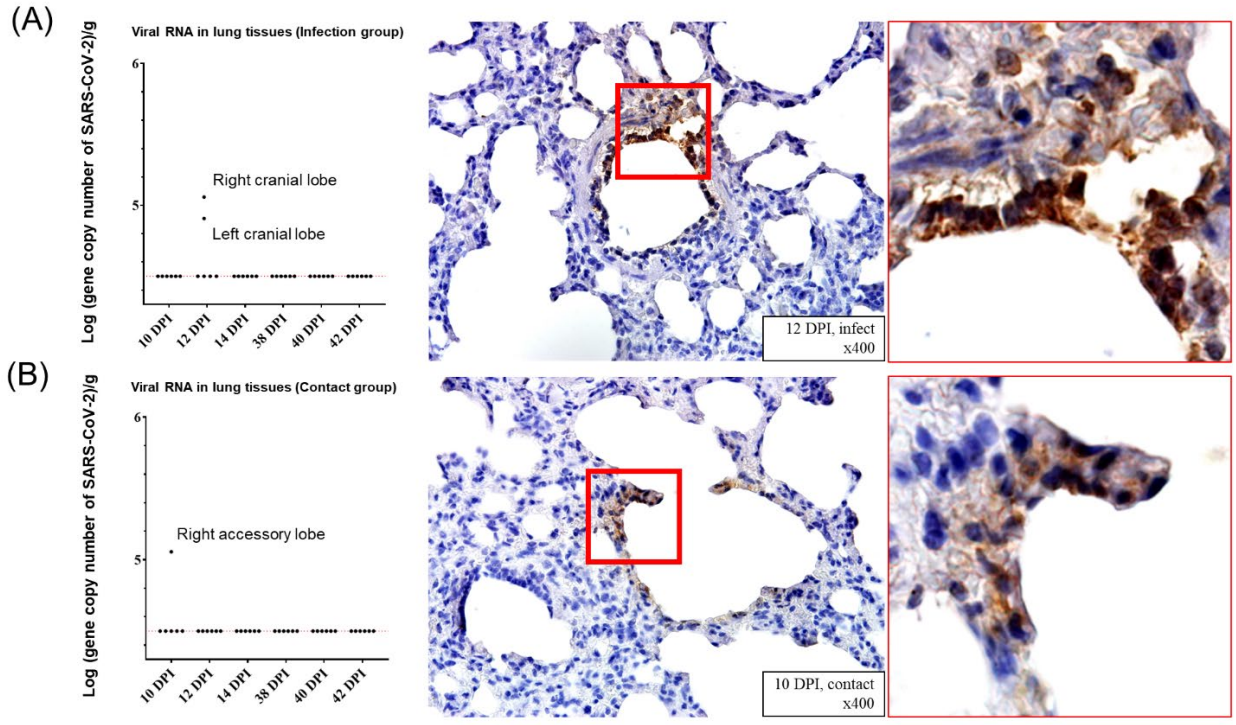


**Appendix Figure 3.** Detection of SARS-CoV-2 RNA in the lung tissues of infected and contact dogs and their immunohistochemistry images. Following autopsy, RT-qPCR was conducted to determine the presence of SARS-CoV-2 in the lung tissues. Among the infection group, two out of 18 early-period lung tissues tested PCR-positive for the virus (A), while one out of 18 early-period lung tissues tested PCR-positive for the virus in the contact group (B). No viral RNA was detected in the late-period tissues. IHC analysis of the PCR-positive tissues confirmed the presence of PCR-positive viral proteins.

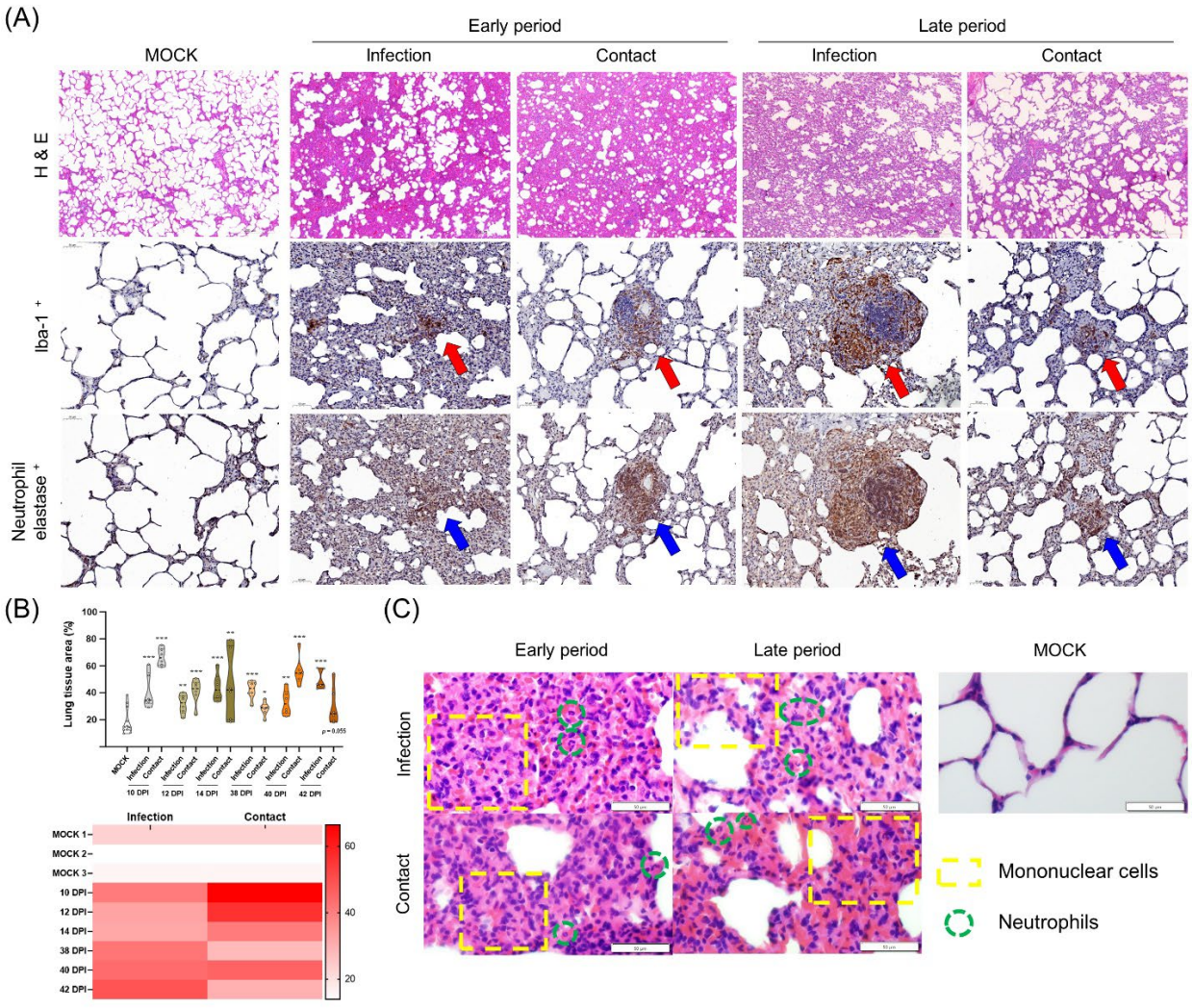


**Appendix Figure 4.** Thickening of the alveolar septa with interstitial pneumonia and infiltration of immune cells. (A) Histopathological changes in the lung tissue of dogs were confirmed through H&E and immunostaining. The H&E staining revealed a thickening pattern of the alveolar septum, while immunostaining showed infiltration of macrophages (red arrow) and neutrophils (blue arrow). (B) Area ratio of the lungs was calculated using the ImageJ program. Data are presented as mean ± SD with a violin plot. *$p < 0.05$, ** $p < 0.01$, and *** $p < 0.001$. (C) The image depicts a close-up view of an alveolar septum that exhibits infiltration of neutrophils (dotted green circle) and mononuclear cells (dotted yellow square).

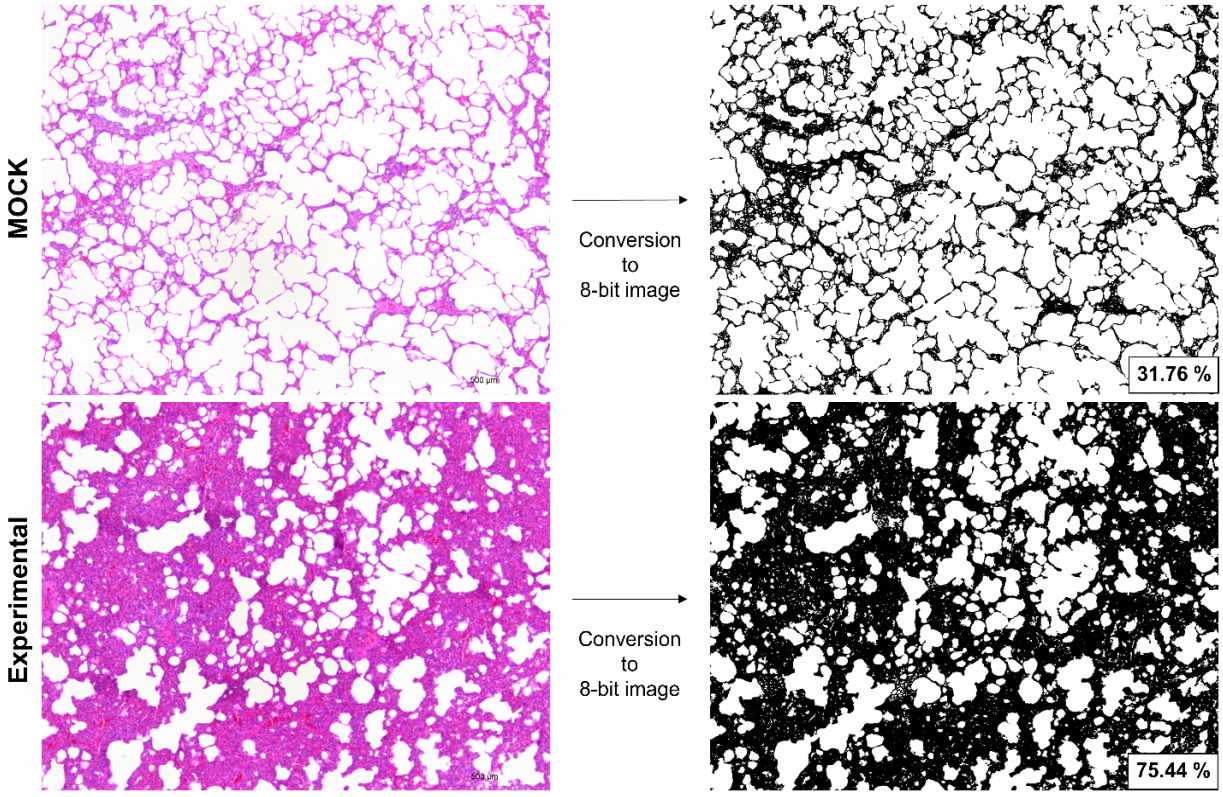


**Appendix Figure 5.** Quantification process of lung tissues by converting to 8-bit images. We randomly selected six parts of the H&E-stained lung tissue slides and compared the ratios with the lung tissue areas. The tissue parts of the lungs were quantified after converting to an 8-bit image. Black parts were digitized using the ImageJ program.

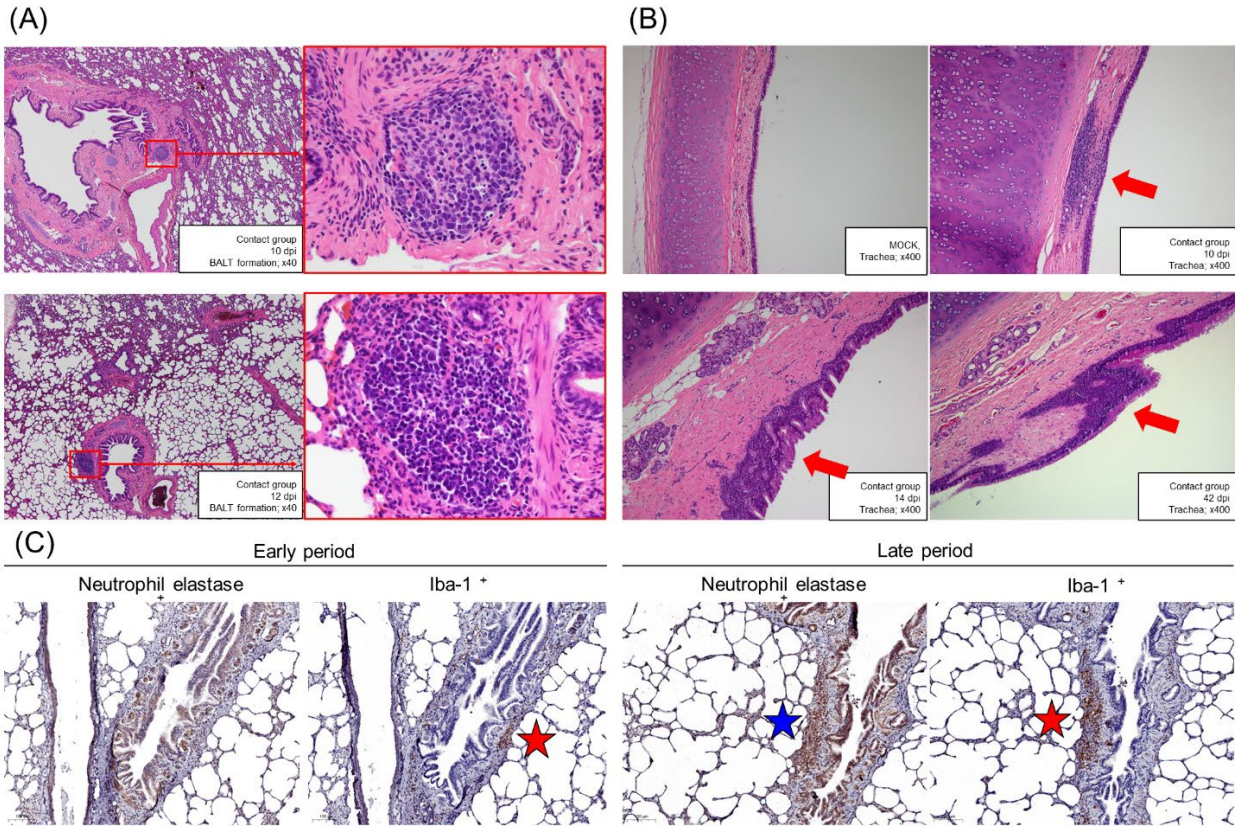


**Appendix Figure 6.** Histopathological changes in the lung tissues of contact dogs. (A) Bronchus-associated lymphoid tissue (BALT) formation was observed during the early infection period in contact dogs. (B) Inflammatory cell infiltration (red arrow) was also observed in the organs of dogs in the contact group during the late stages of infection. (C) In addition to BALT formation, inflammatory cell infiltration was confirmed in the bronchioles. Immunostaining revealed infiltration of neutrophil elastase-positive cells, a marker of neutrophils, during the late period (blue star). Additionally, infiltration of Iba-1-positive cells, a marker of macrophages, was observed during both the early and late infection periods (red star).

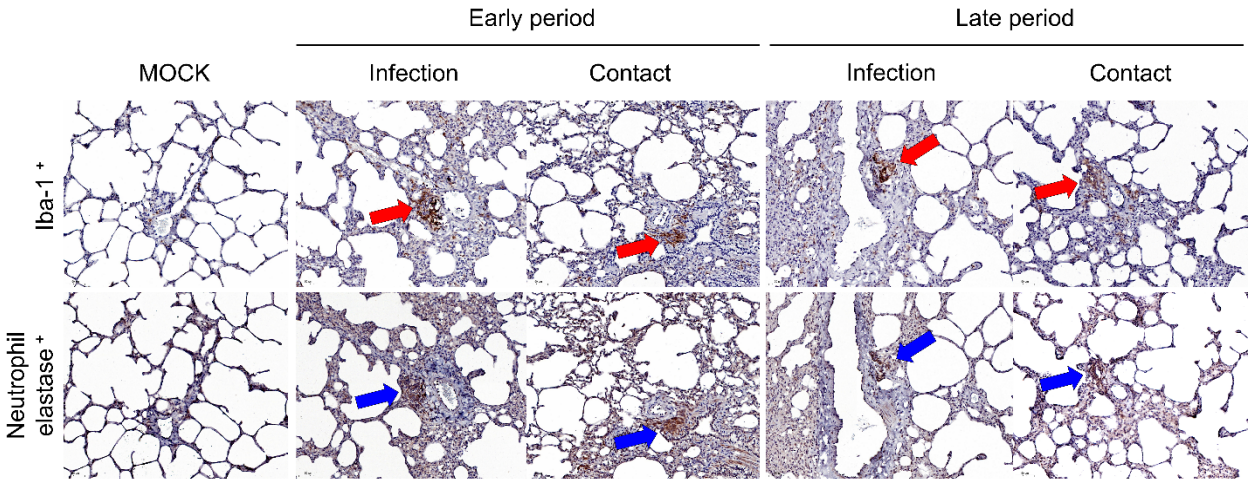


**Appendix Figure 7.** Infiltration of immune cells to adjacent pulmonary blood vessels. Immunostaining revealed infiltration of Iba-1-positive cells (red arrow), a marker of macrophages, and neutrophil elastase-positive cells (blue arrow), a marker of neutrophils, around the pulmonary blood vessels during both the early and late infection periods.

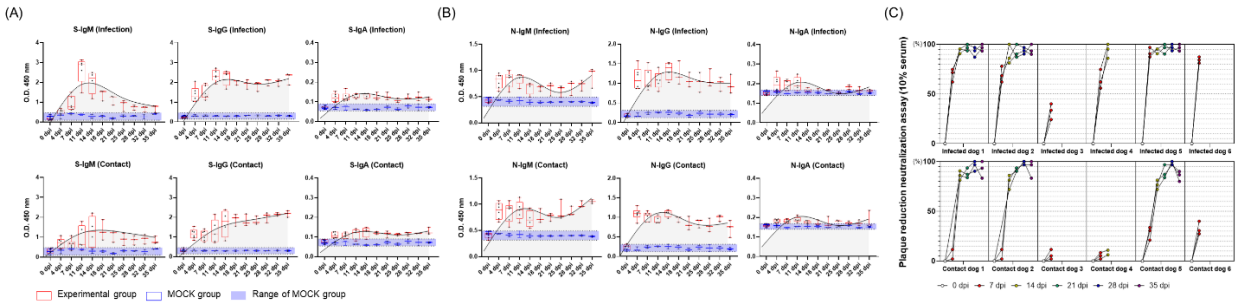


**Appendix Figure 8.** Seroconversion of IgA, IgM, and IgG antibodies to the spike S and nucleocapsid proteins of SARS-CoV-2. After SARS-CoV-2 inoculation, dog blood was collected at regular intervals. The response of IgA, IgM, and IgG antibodies to S protein (A) or N protein (B) in the serum is shown in the box and whisker plots (red box: experimental groups; blue box: MOCK groups). All antibody values detected in uninfected dogs are distributed within the range of the purple box. Smoothing spline curves with four knots were created in 48 segments (black). (C) The formation of neutralizing antibodies in the experimental group of dogs was evaluated using diluted serum (10-fold dilution).

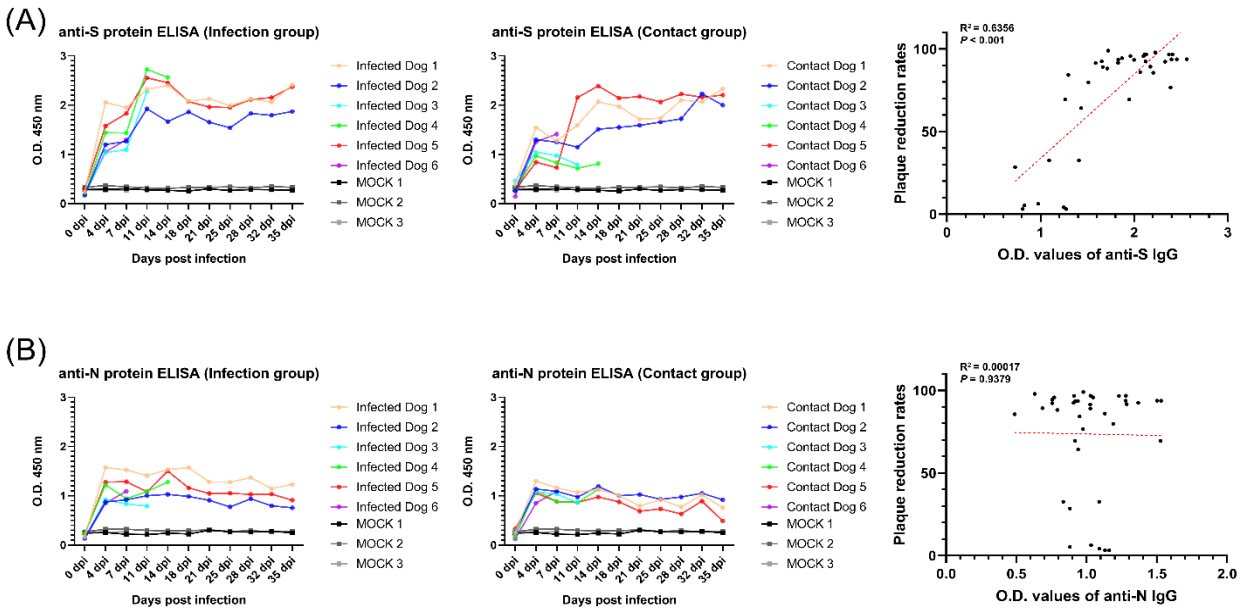


**Appendix Figure 9.** IgG antibody titers of individual dogs after SARS-CoV-2 infection. To determine the relationship between the formation of neutralizing antibodies and the levels of IgG antibodies for each dog (data in Appendix Figure 8), an individual IgG antibody graph and correlation plot between plaque reduction rate and O.D. values of the IgG antibody were generated.

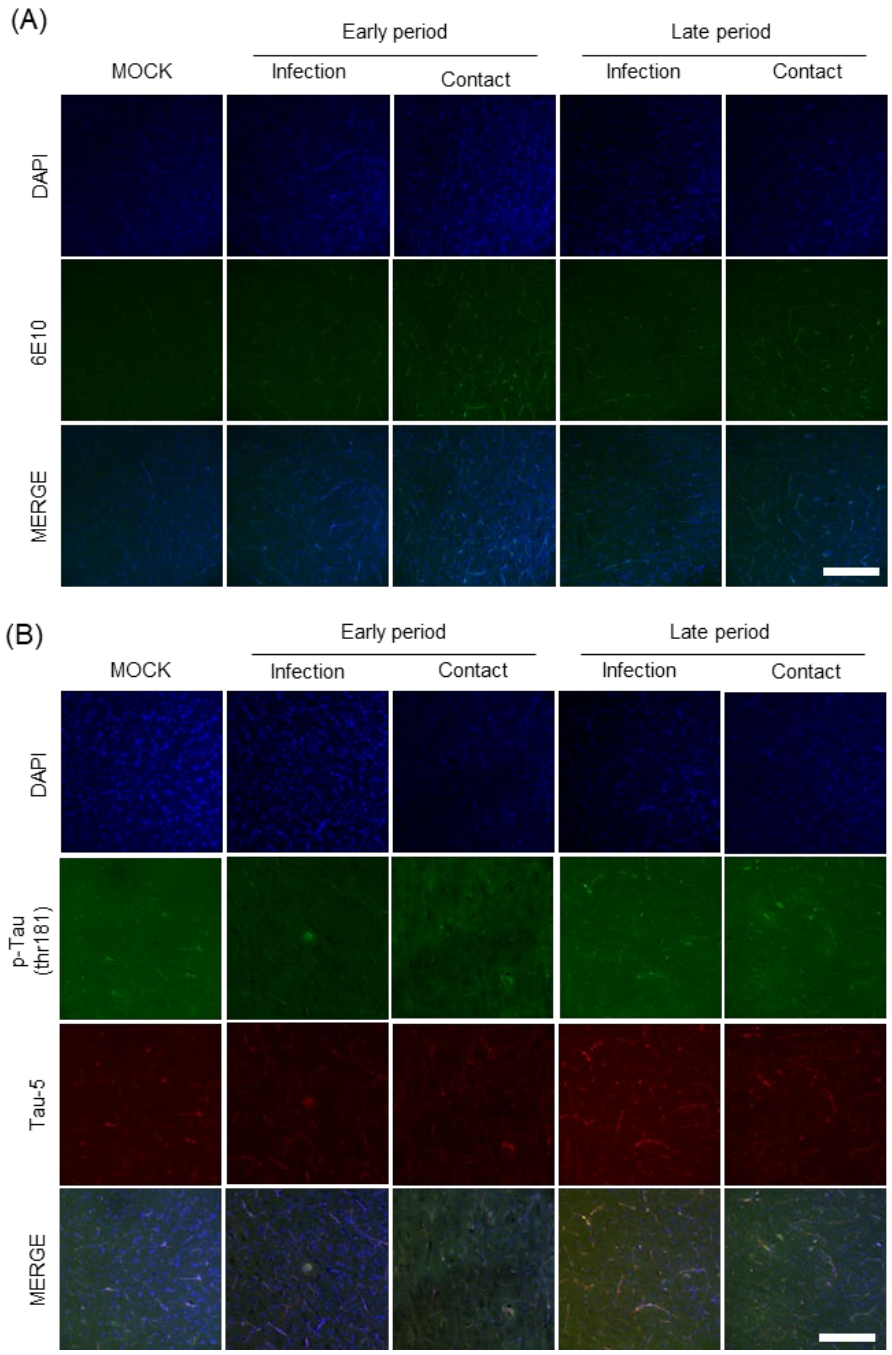


**Appendix Figure 10.** Amyloid β accumulation and Thr181-phosphorylated Tau were not detected in SARS-CoV-2 infected dogs. (A) Representative confocal microscopic images of 6E10 (a marker of amyloid beta, green) staining of canine brain gray matter sections derived from SARS-CoV-2-infected and contact groups at early and late infection periods. (B) Representative confocal microscopic images of phosphorylated Tau (thr181, green) and Tau-5 (total Tau, red) staining of canine brain white matter sections derived from SARS-CoV-2-infected and contact groups at early and late infection periods. The scale bar represents 200 μm.